IUPAC critical evaluation of the rotational–vibrational spectra of water vapor, Part III: Energy levels and transition wavenumbers for $H_2^{16}O$

Jonathan Tennyson [a,*], Peter F. Bernath [b], Linda R. Brown [c], Alain Campargue [d], Attila G. Császár [e], Ludovic Daumont [f], Robert R. Gamache [g], Joseph T. Hodges [h], Olga V. Naumenko [i], Oleg L. Polyansky [a], Laurence S. Rothman [j], Ann Carine Vandaele [k], Nikolai F. Zobov [l], Afaf R. Al Derzi [a], Csaba Fábri [e], Alexander Z. Fazliev [i], Tibor Furtenbacher [e], Iouli E. Gordon [j], Lorenzo Lodi [a], Irina I. Mizus [l]

[a] *Department of Physics and Astronomy, University College London, London WC1E 6BT, United Kingdom*
[b] *Old Dominion University, Norfolk, VA, USA*
[c] *Jet Propulsion Laboratory, California Institute of Technology, Pasadena, CA, USA*
[d] *Université Joseph Fourier, Grenoble, France*
[e] *Loránd Eötvös University, Budapest, Hungary*
[f] *Université de Reims Champagne-Ardenne, Reims, France*
[g] *University of Massachussets, Lowell, MA, USA*
[h] *National Institute of Standards and Technology, Gaithersburg, MD, USA*
[i] *Institute of Atmospheric Optics, Russian Academy of Sciences, Tomsk, Russia*
[j] *Harvard-Smithsonian Center for Astrophysics, Cambridge, MA, USA*
[k] *Institut d'Aéronomie Spatiale de Belgique, Brussels, Belgium*
[l] *Institute of Applied Physics, Russian Academy of Sciences, Nizhny Novgorod, Russia*

ARTICLE INFO

ABSTRACT

This is the third of a series of articles reporting critically evaluated rotational–vibrational line positions, transition intensities, and energy levels, with associated critically reviewed labels and uncertainties, for all the main isotopologues of water. This paper presents experimental line positions, experimental-quality energy levels, and validated labels for rotational–vibrational transitions of the most abundant isotopologue of water, $H_2^{16}O$. The latest version of the MARVEL (Measured Active Rotational–Vibrational Energy Levels) line-inversion procedure is used to determine the rovibrational energy levels of the electronic ground state of $H_2^{16}O$ from experimentally measured lines, together with their self-consistent uncertainties, for the spectral region up to the first dissociation limit. The spectroscopic network of $H_2^{16}O$ contains two components, an ortho (o) and a para (p) one. For o-$H_2^{16}O$ and p-$H_2^{16}O$, experimentally measured, assigned, and labeled transitions were analyzed from more than 100 sources. The measured lines come from one-photon spectra recorded at room temperature in absorption, from hot samples with temperatures up to 3000 K recorded in emission, and from multiresonance excitation spectra which sample levels up to dissociation. The total number of transitions considered is 184 667 of which 182 156 are validated: 68 027 between para states and 114 129 ortho ones. These transitions give rise to 18 486 validated energy levels, of which 10 446 and 8040 belong to o-$H_2^{16}O$ and p-$H_2^{16}O$, respectively. The energy levels, including their labeling with approximate

normal-mode and rigid-rotor quantum numbers, have been checked against ones determined from accurate variational nuclear motion computations employing exact kinetic energy operators as well as against previous compilations of energy levels. The extensive list of MARVEL lines and levels obtained are deposited in the supplementary data of this paper, as well as in a distributed information system applied to water, W@DIS, where they can easily be retrieved.

1. Introduction

Water is the most abundant polyatomic molecule in the universe and it is responsible for the majority of the greenhouse effect on Earth [1]. As a result, the spectrum of water vapor is one of the most thoroughly studied [2]. Topical reviews are available from both experimental [2,3] and theoretical [4,5] perspectives. The need for highly-accurate levels and lines of water vapor is emphasized by articles in the recent volume of "Water in the gas phase" [6]. As for astrophysics, lines and levels are crucial to interpret maser sources [7–9], comets [10], planets [11], exoplanets [12], cool stars [13], carbon stars [14], and interstellar clouds [15,16]. Critically-evaluated energy levels are also useful for a variety of scientific and engineering applications, see, for example, the introduction of Ref. [17], including determining partition functions and hence thermodynamic data [18], and the refinement of theoretical models. Water vapor also plays an important role in characterizing combustion systems [19].

The first 13 authors of this paper form a Task Group under the auspices of IUPAC (International Union of Pure and Applied Chemistry), with the aim of constructing a database of water transitions from experiment and theory, and with individual tasks described in Table 1 of the first paper in this series [20], henceforth referred to as Part I. Since absorption due to electronic excitation requires energies over $50\,000\,\mathrm{cm}^{-1}$ in the case of the water molecule, most of its physical properties are determined by its ground electronic state [21]. This determines the nature of water spectroscopy [2], and thus the present effort concentrates on the pure rotational and rovibrational energy levels of water from within the ground electronic state. We consider all the corresponding transitions up to the first dissociation limit of the molecule simultaneously and on an equal basis.

This paper is the third in a series presenting our evolving methods for collecting and analyzing the experimental (spectroscopic) and quantum chemical information available as well as our validated data recommended for deposition in information systems. In Part I [20], we derived labeled energy levels and transition wavenumbers for the water isotopologues $H_2^{17}O$ and $H_2^{18}O$. In Part II [22], we derived labeled energy levels and transition wavenumbers for the partially deuterated water isotopologues $HD^{16}O$, $HD^{17}O$, and $HD^{18}O$. These analyses were based on the concept of spectroscopic networks [23,24] and were executed using the MARVEL (Measured Active Rotational–Vibrational Energy Levels) protocol of Furtenbacher and Császár [23,25–27], which was considerably refined during the course of the present study [27]

to allow for the treatment of large datasets. Within the MARVEL analysis, a significant amount of checking is performed in order to minimize inconsistencies and errors in the experimental transition data.

In this work we apply the MARVEL algorithm and code to the main $H_2^{16}O$ isotopologue of the water molecule. Unlike the other isotopologues of water, the energy levels of $H_2^{16}O$ were already subjected to a comprehensive and systematic study by Tennyson et al. [28]. We note, for example, that the recent release of the HITEMP database [29] used the energy levels of Ref. [28] to generate transition wavenumbers for hot-water spectroscopy. The present study significantly improves on the methodology used previously [28] and, given a decade of further collection of experimental data, considerably extends its scope. In this context we note in particular the multi-resonance studies of Boyarkin, Rizzo, and co-workers, which have probed the energy levels of water up to [30–34] and even beyond [35] the first dissociation limit. These sophisticated experiments have sparked corresponding theoretical studies [34,36,37]. Here we consider all the available experimental spectroscopic transition data linking rotation-vibration levels below the first dissociation limit of $H_2^{16}O$.

As emphasized already in Parts I and II, a distinguishing feature of the present series of IUPAC-sponsored spectroscopic studies is the joint utilization of all available experimental and the best theoretical line (transition) and energy-level data, with a long-term aim of creating complete linelists for all water isotopologues. While determination of a complete linelist is outside the scope of present-day experiments, it can be determined by means of sophisticated first-principles quantum chemical computations. Studies on the spectroscopic networks of water isotopologues [24,38] also revealed that a large number of energy levels participate in some transitions strong enough to be observable. Thus, although only a small portion of all the allowed transitions will ever be observed experimentally, it seems likely that the majority of energy levels will eventually be connected to observed transitions. For the time being, as experimental line positions have a higher accuracy than those yielded by even the most advanced computations, complete linelists will necessarily contain a mixture of accurate experimental data and less accurate computational data. MARVEL-type efforts (a) replace as many computed lines as possible with their experimental counterparts, (b) validate and ideally reduce the uncertainty with which a transition has been determined, and (c) facilitate the assignment of experimental spectra. Unlike line positions, the overwhelming majority of one-photon, temperature-dependent absorption and

emission intensities can be computed with an accuracy matching or even exceeding most of the measurements. Thus, the availability of first-principles intensities, based on computed and perhaps empirically adjusted potential energy surfaces (PES) [39–46] and dipole moment surfaces (DMS) [47–49], greatly helps in the assignment and labeling of experimental absorption or emission spectra.

2. Methods, input data, and data treatment

The methods employed in this study for collecting and critically evaluating labeled experimental transition wavenumbers and their uncertainties and for inverting the wavenumbers in order to obtain the best possible energy levels with corresponding uncertainties are principally based on the concept of spectroscopic networks [23,24] and on the MARVEL procedure [23–27]. During a MARVEL analysis we simultaneously process *all* the available assigned and labeled experimental lines to give the associated energy levels of the chosen isotopologue. We adopted a reweighting scheme [51] where uncertainties for selected line positions are changed (in practice increased) during iterations of the MARVEL procedure [25]. After removing outliers from the experimental transition data and applying the iterative robust reweighting algorithm, a database is created containing self-consistent and uniquely labeled transitions and related uncertainties. The procedure is such that the final energy levels and their uncertainties are guaranteed to be compatible with the (adjusted) uncertainties of the experimental line positions. This means that all transitions used in the MARVEL procedure agree, within their revised stated uncertainties, with the MARVEL predictions. This criterion for the error is therefore more stringent than the usual standard deviation used to represent statistical error and will usually lead to the quoted MARVEL errors being systematically larger.

The first step in the MARVEL procedure is to split the transition data into components of the spectroscopic network (SN) characterizing the molecule [24]. Components of SNs contain all interconnected rotational–vibrational energy levels supported by the grand database of the labeled transitions. For $H_2^{16}O$, the transitions must form two rooted components, an ortho and a para one (Table 1). Other components of the SN whose nodes are unattached to either of the two roots are designated as floating spectroscopic networks (FSNs) or, in the case of a single transition with no energy level in common with any of the other transitions in the compilation, orphans (ORPs). The selection rules for electric-dipole-allowed transitions are as follows: within

the ortho or para SNs transitions are allowed if $\Delta J = \pm 1$ and $\Delta p = 0$ or $\Delta J = 0$ and $\Delta p = 1$, where J is the quantum number describing the overall rotation of the molecule and p is defined in the footnote to Table 1.

For $H_2^{16}O$, there exists an unusually large number of at least partially assigned experimental spectra [17,28,30,33–35, 52–165].The data from room-temperature spectra are augmented by data from a number of warm (400–700 K) and hot (up to 3000 K) $H_2^{16}O$ spectra [83,93,94,96–98,107, 124,135,148,164,166–177]. Hot spectra are rich in high-J and hot-band transitions but often have significantly larger uncertainties and a much increased chance of misassignment and mislabeling. Another significant feature of water spectroscopy is that the spectrum has been probed by multiresonance experiments up to [30–34] and even beyond [35] the first dissociation limit of the molecule. These studies significantly extend our knowledge of the ground electronic state of the water molecule. Some of the papers on water vapor spectra report only intensity or lineshape data and are therefore not employed in a direct fashion in this study.

Measured spectra of $H_2^{16}O$ vapor are basically a superposition of two separate spectra, that of ortho-water and para-water (Table 1), the strongly forbidden transitions between the two spin isomers have never been observed [178]. Lines of ortho-water (total spin of protons $I=1$) exhibit, under ultrahigh resolution, hyperfine structure (*hfs*) due to the coupling of the proton nuclear spins with the rotational angular momentum (*i.e.*, interaction between the magnetic moments of the protons and the magnetic field generated by the molecular rotation) and to a direct spin–spin interaction. All ortho-water levels with $J > 0$ are split into three *hfs* components with $F = J-1, J$, and $J+1$, where $\mathbf{F} = \mathbf{J}+\mathbf{I}$ is the total angular momentum of the system. The "center of gravity" of the levels and associated lines is not shifted due to this splitting. The spectrum of para-water ($I=0$) exhibits no *hfs*. There are several papers on water spectroscopy which addressed the *hfs* splittings [7,61,145,159]. The accurate and precise unperturbed frequencies reported in these papers are highly useful for the present study. However, since *hfs*-resolved data exist only for a few levels, we work with the (*hfs*-averaged) line centers. Since the separation between ortho and para states is not measured experimentally, it is necessary to fix it using a so-called magic number. This was done by setting the energy of the (0 0 0) [1 0 1] state to 23.794352 cm^{-1}, the number determined by 01LaCoCa [124] using an effective Hamiltonian. This "magic number" was supported, to the given number of digits, by a MARVEL analysis of the final energy levels whereby the degeneracy between a large number of ortho and para levels was introduced to couple the two SNs.

There are several papers, *e.g.*, Refs. [28,135,137], which report many derived energy levels but no or few original experimental transitions. The energy levels of $H_2^{16}O$ have been studied using several theoretical schemes. As the usual effective Hamiltonian approach is problematic for water [179], several simple theoretical approaches have been developed and tried on water spectra, including the Padé approximation [179–181], the Borel approximation [90,137,179], generating functions [39,182,183], joint perturbational-variational approaches [184], and

Table 1
Symmetry characteristics of the rotational–vibrational states of $H_2^{16}O$.[a]

Symmetry	A_1	A_2	B_1	B_2
Parity	+	−	−	+
ortho/para (O/P) state	P	P	O	O

[a] Parity $= (-1)^{(J+p)} = (-1)^{K_c}$, where p is defined as 0 for e and 1 for f states [50]. The ortho and para labels are defined by $(-1)^{v_3+K_a+K_c}$. See Section 2 for the meaning of the approximate vibrational and rotational quantum numbers.

Table 2
Data sources and their characteristics for $H_2^{16}O$.[a]

Tag	Range (cm^{-1})	Trans. A/V	Physical conditions				Comments (see Section 2.7)
			T (K)	p (hPa)	Rec.	L (m)	
79HeJoMc [73]	0.072–1677.21	3/3	RT		SMM		
91PeAnHeDe [94]	0.072–19.804	31/31	1400	0.13	MME-SHW	1.5	(2a)
06MaToNaMo [146]	0.072–165.310	130/130	300–900	0.01–0.6	LDFS	1.8	
80Kuze [75]	0.401–4.003	4/4	473	3.9	MW-BWO	1.5	
69Kukolich [56]	0.742	1/1	RT				
72FlCaVa [60]	0.742–25.085	7/7	RT	0.13–13		> 5	
81Kyro [77]	0.742–25.085	15/15			FTS		
71StBe [58]	2.262	1/1	RT				
00ChPePiMa [119]	4.330–52.511	25/25	RT	0.13		1	(2b)
54KiGo [53]	6.115	1/1	RT		MMW	0.2	
71Huiszoon [57]	6.115	1/1	RT		MMW	0.4	
06GoMaGuKn [145]	6.115–18.577	13/13	RT	0.13	LD		(2c)
87BeKoPoTr [90]	7.762–19.850	5/5	RT	0.26, 1.3			(2d)
91AmSc [93]	8.254–11.835	5/5	438		MMW	1.5	(2e)
12YuPeDrMa [164]	9.796–694.486	4510/4501	RT,hot	< 18	EMS-FTS	0.3–2	(2f)
72DeHeCoGo [59]	10.715–25.085	13/13	RT		SMW	0.3	
09CaPuHaGa [159]	10.715–20.704	7/7	RT	0.00013–0.00065	LD	3	
83HeMeDe [82]	13.013–32.954	7/7	RT			1	(2g)
87BaAlAlPe [89]	14.199–19.077	6/6	1300		MW-BWO	2.2	
83BuFeKaPo [80]	16.797–21.545	5/5	RT	1.3	SMW		
81Partridg [78]	16.799–47.055	26/26	RT	1.3–21	FTS	< 12	(2h)
95MaOdIwTs [104]	18.577–162.44	139/139	RT	0.047	LDFS	0.5	(2i)
85Johns [86]	18.578–349.76	261/261	RT	< 2.6	FTS	0.15	
78KaKaKy [70]	32.955–713.80	417/417	RT	0.5–5	FTS	1	(2j)
09CaPuBuTa [158]	36.604–53.444	15/15	297	0.005–1.57		0.01	
04CoPiVeLa [135]	58.019–475.09	1708/1708	1850	1	EMS-FTS	1	(2k)
11DrYuPeGu [162]	82.862–90.843	26/26	RT	0.0013–0.4		2.2	(2l)
97DeLoInNo [109]	118.32–119.07	5/5	RT	0.02–0.6	EMS	0.32–0.4	
95PaHo [105]	177.86–519.59	246/246	295	0.5	FTS	3.2	(2m)
05HoAnAlPi [138]	212.56–594.95	166/166	RT	0.0013–4.1	FTS	10,16,42	(2n)
97PoZoViTe [168]	373.65–933.62	3379/3270	1823	1	EMS-FTS		(2o)
97PoTeBe [167]	385.08–874.26	400/398	1823		EMS-FTS		(2p)
96PoBuGuZh [107]	407.31–921.40	586/556	1823	20	EMS-FTS		(2q)
82KaJoHo [79]	501.57–713.79	71/71	RT	2.5	FTS	1	(2r)
05CoBeCaCo [174]	539.55–1999.76	11 406/11 140	3000		EMS-FTS		(2s)
98Toth [113]	590.60–851.25	49/49	295–302	0.7–3.5	FTS	0.25–433	
05ZoShPoTe [175]	614.45–1893.87	160/110	3000		EMS	1013	(2t)
98EsWaHoRo [170]	720.10–1397.84	751/750	1000	26	EMS-FTS		(2u)
06ZoShPoBa [176]	722.04–4749.92	15 984/15 721	3000		EMS-FTS		(2v)
92MaDaCaFl [98]	811.57–1265.07	80/80	2000		EMS-FTS		(2w)
92DaMaCaFlb [97]	855.91–1848.81	216/214	2000		EMS-FTS		(2x)
97PoZoTeLo [169]	928.68–2323.72	1544/1539	1273	1.18	EMS-FTS		(2y)
99ZoPoTeLo [171]	933.37–2500.29	6774/6706	1823	8	EMS-FTS		
99Toth [114]	995.98–4488.60	3143/3142	RT		FTS		(2z)
01ByNaSiVo [123]	1027.5–14 139.2	156/153					(2aa)
83Guelachv [81]	1066.2–2296.7	1177/1177	RT	0.013–1.26	FTS	16–44	(2bb)
91Toth [95]	1066.2–2582.6	1011/1007	296–298	0.023–17.26	FTS	0.08–434	(2cc)
92DaMaCaFla [96]	1092.5–1844.0	159/158	2000		EMS-FTS		(2dd)
93Totha [99]	1304.3–4260.4	889/886	RT	0.39–18.1	FTS	2.4–434	(2ee)
85BrTo [84]	1323.3–1992.7	71/71	RT		FTS		(2ff)
93Tothb [100]	1820.8–4506.2	2316/2315	296	0.44–17.2	FTS	2.4–434	
97MiTyKeWi [110]	2507.2–4402.8	940/920	296–298	0.063–19.5	FTS	3–288	(2gg)
05Toth [140]	2926.5–7640.8	1896/1895	RT	1.3–19.5	FTS	1.5–433	(2hh)
73CaFlGuAm [62]	2933.7–4250.9	1316/1312	RT	1.33	FTS	8	(2ii)
83PiCoCaFl [83]	2966.0–4004.7	2656/2406	1200	1–2.6	LDFS	1	
73PuRa [64]	3261.0–4193.9	34/23			GRS		(2jj)
02MiTyStAl [127]	4200.1–6241.8	4078/4078	297–298	0.1–3.0	FTS		
07JeDaJaTy [150]	4200.1–6599.7	5421/5418	RT	2–23	FTS	0.3–1230	
77FlCaMaGub [69]	4200.2–5554.9	448/447	333	120	FTS	40	
02TeBeZoSh [173]	4253.8–7552.5	6019/6013	1800		EMS-FTS		(2kk)
08ZoShOvPo [177]	4253.8–12 361.4	26 106/25 490	3000		EMS-FTS		(2ll)
86GuRa [192]	5103.3–5547.1	234/234					
96BrMa [106]	5206.3–5396.5	28 /28	RT		FTS		
94Tothb [103]	5750.9–7987.5	3808/3808	296–298	1.3–19	FTS	2.4–433	
09LiNaKaCa [160]	5908.7–6725.7	1165/1165	RT	0.13–13.3	CRDS	NR	(2mm)
07MiLeKaCa [152]	5912.6–7014.9	1245/1241	296	1.5–20	CRDS	NR	(2nn)
80CaFlMa [74]	5937.4–6443.1	80/80	333	120	FTS	40	(2oo)

Table 2 (continued)

Tag	Range (cm^{-1})	Trans. A/V	Physical conditions				Comments (see Section 2.7)
			T (K)	p (hPa)	Rec.	L (m)	
04MaRoMiNa [136]	6131.4–6748.6	2364/2353	RT	22.3	CRDS	NR	
86MaChCaFl [88]	6443.1–7830.3	379/369	300	1.97	FTS	434	
12LeMiMoKa [165]	6885.8–7405.9	2518/ 2516	296.4	0.13–0.40	CRDS	NR	
75ToMa [67]	6952.3–7508.4	882/796	RT	1.33–12	GRS	8–32	(2qq)
11MiKaWaCa [163]	7408.2–7919.2	2010/2010	RT	1.3–13.3	CRDS	NR	(2rr)
05ToTe [141]	7423.7–9595.4	4235/4205	294.4	20.08	FTS	480.0	(2ss)
88MaChFlCa [152]	8057.9–9481.8	1667/1663	300	2.0–22.8	FTS	433.96	(2tt)
75FlCaNaCh [66]	8060.1–9366.6	1125/1111	296/333	9.3/120	GRS/FTS	100/40	(2uu)
05ToNaZoSh [142]	9155.1–25 224.9	15 566/15 432	292	6–18	FTS	600	(2vv)
06PePoSeSi [148]	9387.8–9451.2	96/86	800, 200		ICLAS		
08ToTe [155]	9502.0–14 495	10 587/10 513	295–296	9–21	FTS	5–512	(2ww)
03NaCa[132]	9518.9–10 009	634/632	298	26.3	ICLAS	33 000	(2xx)
89ChMaFlCa [92]	9603.7–11 480	2394/2391	300	2.0–22.8	FTS	433.96	(2yy)
02BrToDu [126]	9676.9–11 383	2594/2579	295–297	3–21	FTS	2.4–434	(2zz)
09GrBoRiMa [34]	10 305–14 619	455/422		NR	MRE	NR	(2aaa)
08LiHo [156]	10 671–10 835	11/9	296	5.5–10.4	CRDS	NR	
06MaNaKaBy [147]	11 335–12 843	1185/1165	RT	2–20	ICLAS	9600–19 200	(2bbb)
97FlCaByNa [193]	11 523–12 837	1642/1639	297	2.0–22.6	FTS	434	(2ccc)
94Totha [102]	11 610–12 752	745/745	297	1.5–21.4	FTS	98–433	(2ddd)
02ToTeBrCa [130]	11 787–13 553	1906/1825	296	21.15	FTS	800.8	(2eee)
08CaMiLi [157]	12 746–13 558	1116/1086	RT	2.20	ICLAS	≤ 23 900	(2fff)
99CaJeVaBe [116]	13 185–21 390	5622/5598	294	18.5	FTS	602.3	(2ggg)
98PoZoViTe [115]	13 239–15 995	2544/2535	300	1.97	FTS	434	(2hhh)
05KaMaNaCa [143]	13 312–13 378	271/255	RT	22.36	CRDS	NR	(2iii)
08GrMaZoSh [33]	13 531–17 448	431/414		NR	MRE	NR	(2jjj)
11BeMiCa [161]	13 542–14 073	174/167	RT	15.8	ICLAS	23 900	(2kkk)
00BrPl [118]	13 818–13 932	7/7	RT	5.2–14.4	FTS	97–193	
85CaFlMaCh [85]	16 548–25 173	991/988	300	2.0–24.5	FTS	434	(2lll)
00ZoBePoTe [120]	21 410–25 225	282/277	291	18.5	FTS	602.3	(2mmm)
05DuGhZoTo [144]	25 196–25 337	47/46	RT	13	CRDS	NR	(2nnn)

[a] The tags listed are used to identify experimental data sources throughout this paper. The range given represents the range corresponding to validated wavenumber entries within the MARVEL input file and not the range covered by the relevant experiment. Uncertainties of the individual lines can be obtained from the supplementary data. Trans.=transitions, with A=number of assigned transitions in the original data source, V=number of transitions validated in this study. T=temperature (K), given explicitly when available from the original publication, with RT=room temperature. p=pressure (hPa). Rec.=experimental technique used for the recording of the spectrum, with GRS=grating spectrometer, EMS=emission spectroscopy, SMM=Stark-modulated microwave spectrometer, FTS=Fourier transform spectroscopy, ICLAS=intracavity laser absorption spectroscopy, CRDS=cavity ringdown spectroscopy, LD=Lamb dip, LDFS=laser difference frequency spectroscopy, MW-BWO=microwave spectrometer with backward wave oscillator, MMW=millimeter wave spectroscopy, SMW=submillimeter-microwave spectrometer, and MRE=multiresonance experiment. NR=not relevant.

a four-dimensional bending–rotation Hamiltonian [185,186]. Due to the assumed simplicity of the water molecule, it has also been a favorite subject of variational nuclear motion computations [34,36,37,39,42–45,47–49,187].

Table 2 provides, for each transition data source, experimental information related to the spectra. The number of originally measured and assigned (A) and validated (V) transitions for each data source is given there, as well. Due to the large amount of related experimental studies, a nearly continuous coverage has been achieved for $H_2^{16}O$ up to about 15 000 cm^{-1}, significantly above the barrier to linearity of the molecule [175,188–190], with transitions sporadically observed beyond this value.

To be included in our tabulation, data sources must include original experimental line positions with uncertainties and line assignments with labels. Information on the conditions under which the experimental data were recorded is summarized in the column 'Physical conditions' in Table 2. As in Parts I and II, the data source is identified with a tag based on the year of publication and the names of the authors (see Part I for more details).

It is important to make a distinction between resolution of the spectrometer and uncertainty of the lines. Often uncertainties can be 10–15 times smaller than the resolution.

Most of the spectra were obtained in absorption by Fourier transform spectroscopy (FTS), which has allowed a wide spectral coverage from the microwave region through the visible to the near ultraviolet. In order to detect weak lines, FTS spectrometers have been equipped with long multipass cells. Absorption path lengths as large as 433, 801, and 1804 m have been achieved with the cells available at Kitt Peak, Rutherford Appleton Laboratory, and University of Reims, respectively, providing a large number of observed transitions in the near infrared and visible regions (up to 26 000 cm^{-1}).

Laser-based methods, such as CRDS (cavity ringdown spectroscopy) and ICLAS (intracavity laser absorption spectroscopy), are limited to certain spectral regions depending on the availability of tunable laser sources. These techniques have specific advantages in terms of sensitivity and spectral resolution, which make them

particularly suitable for the characterization of spectral regions with weak absorption features. This is why extensive investigations with laser-based methods were mostly limited to transparency windows or to the visible region. The precision of CRDS is limited to about 0.001 cm^{-1}.

Emission spectra can provide large datasets of line positions. Emission spectra for water are available over a particularly extensive range of temperatures, the hottest being spectra recorded in an oxy-acetylene flame at about 3000 K [174]. These spectra provide a rich source of information on states both with significant bending excitation [175], which are normally not probed in standard absorption spectra, and with high levels of rotational excitation. Hot spectra suffer from the disadvantage that it is not usually possible to obtain line positions with the same accuracy as spectra recorded at room temperature. This is due to the increased Doppler width of the transitions and, in the case of atmospheric pressure spectra such as those recorded in flames, significant pressure broadening and pressure shifts. The extended linewidths and high density of transitions also leads to very large numbers of blended transitions, which places a further constraint on the accuracy with which the positions of the individual lines can be determined. It should be noted that absorption spectra recorded in sunspots correspond to a temperature of about 3200 K [191], close to the hottest laboratory emission spectra. Sunspots provide a very rich source of spectroscopic data on water [168] and many lines, which are almost certainly due to hot water, still need to be assigned.

2.1. Pre-MARVEL validation

Similar to Parts I and II, the experimental database assembled based on literature data were first checked for simple transcription errors or other problems in the original data source. Checks were made for formatting incompatibilities, entries with zero uncertainties (not allowed in a MARVEL-type analysis), strongly forbidden (ortho to para) transitions, and transitions with impossible labels. As to invalid labels, the dataset of transitions was searched for cases where the $K_a + K_c$ sum, where K_a and K_c are the usual asymmetric-top rigid-rotor quantum numbers, did not equal J or $J+1$, where J is the rotational quantum number, where either K_a or K_c were greater than J.

A search was performed to identify obvious duplications in the dataset in order to avoid entering the same measurement twice. A warning was issued if this happened and only the earliest occurrence of the datum was kept (unless the line was reanalyzed in a later study). We also made sure that the dataset of transitions to be analyzed by MARVEL did not contain (a) entries where the two transitions had the same lower-level label but different upper-level labels with transition wavenumber differences less than 0.05 cm^{-1}, and (b) where the transitions had the same lower- and upper-level labels and their wavenumbers differed beyond the related uncertainties. Employing the parities detailed in Table 1 and the associated selection rules, transitions which had incompatible labels were identified and deleted. The rotational

parity along with the J values helped in the search for correspondence between the experimental and the variational datasets.

Another pre-MARVEL validation procedure utilized the so-called BT2 linelist [194]. If the BT2 variational nuclear-motion computations indicated the existence of a degeneracy between an ortho and a para transition within the BT2 linelist to better than 10^{-3} cm^{-1} and one of the transitions was missing from the MARVEL input, the missing entry was added by hand and indicated as such in the input by adding the letter "D" to the tag of the duplicated transition entry. We added altogether 6589 duplicates to the original database. This step was important to link a number of what otherwise would have been FSNs.

2.2. Assignment, labels

It is a requirement of the MARVEL protocol that the dataset contains a single unique label for both the lower and the upper states involved in each transition. There is no requirement that labels have any physical significance beyond those needed to give selection rules. Due to the extent of the data for transitions of $H_2^{16}O$, a large number of problems were expected for the approximate vibrational labels. For consistency and to maintain a single set of uniform labels for all levels, we chose to label vibrational states in the usual normal-mode notation, $(v_1 \ v_2 \ v_3)$. There are strong physical arguments that the higher stretching states of water are better labeled using local modes [195,196]. However, there is a one-to-one correspondence between local- and normal-mode labeling schemes [116], so the use of normal-mode labels leads to no loss of information. We have therefore translated assignments given in local modes into normal modes. We note that for a number of data sources it proved necessary to systematically re-label data assigned in normal mode notation as the labels did not map to the correct and very characteristic local mode energy level structure. This issue has been noted previously [116]. In this work we retain, whenever possible, the ordering and the normal-mode labeling of the vibrational states of $H_2^{16}O$ presented and advocated in Ref. [197].

Similar problems arise from the approximate standard asymmetric top quantum numbers $[J \ K_a \ K_c]$, used as part of the label of the rovibrational states. Driven by the required uniqueness of the labels, the rotation–vibration levels of $H_2^{16}O$ are identified in this study by altogether six quantum numbers: $(v_1 \ v_2 \ v_3) \ [J \ K_a \ K_c]$.

Before processing the published transition data, we checked, as thoroughly as possible, whether the transition labels were correct and consistent. For $H_2^{16}O$ several of the older sources permuted labels for a number of higher-lying excited states compared to those advocated here. Where possible, we corrected for this. Rovibrational labels, which could be used for checking the $(v_1 \ v_2 \ v_3) \ [J \ K_a \ K_c]$ labels of the experimental transitions, could be taken from computations based on the use of an effective Hamiltonian (EH). However, for the majority of the high-lying energy levels, results from proper EH computations are not available. Validation of the labels attached to the

observed transitions was thus performed as follows. Transitions were examined for consistency of the upper levels derived from combination difference (CD) relations. This method is a simple and powerful tool for the assignment of rovibrational spectra; however, it cannot be applied to transitions not part of several CD relations. All the transitions associated with a given rotational level of the (0 0 0) vibrational ground state have been considered for combination differences. At this stage, conflicting labels could be traced and corrected. Many CD relations for other rovibrational states have also been checked.

An important check of the labels is provided by the normal-mode decomposition (NMD) and rigid-rotor decomposition (RRD) analyses [198,199] of the variationally computed rovibrational wave functions. This is a powerful technique to identify approximate vibrational and rotational labels based on the harmonic oscillator and rigid rotor formalisms and the rovibrational wavefunctions obtained from variational treatments. Validation of rovibrational labels with J less than 26 has been attempted by computing RRD tables. For obtaining RRD labels, a cut-off value of 0.7 was chosen for the largest RRD coefficient, i.e., only cases where the labeling is unambiguously provided by the RRD scheme were utilized. Rovibrational states with an energy larger than $25\,000\,cm^{-1}$ were also not investigated since for them there appear to be very few states which can clearly be labeled via an RRD table. This means that for a large number of MARVEL energy levels no validation via the RRD scheme was attempted. The extent of validated labels for the different vibrational band origins (VBO) is given in Table 3, which also gives the J_{max} values (the maximum J value on the particular VBO) for a large number of VBOs. Clearly, it is more problematic to provide unambiguous rotational labels for VBOs which contain a high level of bending excitation. In particular, starting from the (0 10 0) VBO no rotational labels on pure bending VBOs could be provided by the RRD methodology; this problem is almost certainly associated with the rearrangement of the energy level structure caused by the monodromy point at linearity [175,200]. In general, as the energy of excitation increases, the highest J value where RRD can be used to validate the MARVEL labels decreases.

Finally, consistent labeling has been established for all the assigned transitions considered. We recommend that the labeling provided in this paper should be generally adopted, although in cases of strongly perturbed energy levels there is considerable remaining uncertainty. In particular, the approximate normal-mode labels, and at higher energies, and especially for high K_a levels, the rigid-rotor labels [198,199], are not expected to provide a physically correct description.

2.3. Uncertainties

Within the MARVEL protocol, reasonable estimates for the accuracy of the observed transitions must be provided. Despite the adjustments by the robust reweighting scheme, due to the existence of a huge number of cycles of various size within the SN of $H_2^{16}O$, false uncertainties attached to the transitions can noticeably deteriorate the accuracy of a large number of MARVEL energy levels.

In some of the data sources, approximate experimental uncertainties are not given for each individual transition. Often only the general accuracy of the transitions for the region investigated is provided. For a few publications we were forced to estimate the experimental uncertainties. If no values were presented in the original source, these uncertainties were based on average values characteristic of the experimental setup exploited in the measurement. We note also that sometimes the experimental uncertainty attached to a line in the original source reflects the quality of the line profile fit rather than the real accuracy with which the wavenumber was determined. For further important adjustments of the uncertainties of transitions of certain data sources see Section 2.7.

MARVEL may increase, via robust reweighting, the assumed experimental uncertainty of a transition when it is not consistent with the one derived from the MARVEL energy levels. For transitions with low J and K_a values it is rather easy to evaluate a feasible experimental uncertainty if enough CDs are available. However, for increased values of J and K_a, the CD relations become less accurate and instructive, a number of experimental lines represent unresolved multiplets, and it becomes more and more difficult to judge properly the actual experimental accuracy of the transitions. This in turn limits the accuracy of the MARVEL energy levels derived. This situation could be improved only by including additional accurate experimental information in the MARVEL input file.

For a number of transitions which proved to be clear outliers, the experimental uncertainties were increased manually (see Section 2.7). This was done when the energy of an upper state deviated far more from the corresponding mean value established by MARVEL than the stated experimental uncertainty. It is our hope that by a computerized search and a subsequent manual adjustment, at least the majority of clear outliers have been identified and either removed from further analysis or were included with a more reasonable uncertainty.

2.4. Hot transitions

The high-lying rotational levels probed by hot transitions are hard to validate due to the high density of both predicted and observed transitions. In addition, some of the transitions to a given upper level originate from lower (sometimes unknown) levels belonging to excited vibrational states.

The most significant problem with the existing hot-water transition data were their inconsistent labeling. Thus, the labels from these data sources were carefully checked once the MARVEL energy levels, and their labels, were well established based on cold water spectra. As the comments to Table 2 (Section 2.7) demonstrate, a large number required careful relabeling so that only a small number of assigned transitions were actually omitted during the final MARVEL runs. It must be emphasized again that (a) labels for the hot water transitions may not be physically correct but at least they are unique and consistent as far as the present database is concerned, and

Table 3
Validation of the rotational labels of the rovibrational levels determined by the final MARVEL analysis via the rigid rotor decomposition (RRD) protocol [198,199], the vibrational band origins (VBOs) are listed in order of increasing energy.[a]

VBO	J_{max}	J_v	No. validated	No. without validation
(0 0 0)	42	23	581	95
(0 1 0)	39	14	475	201
(0 2 0)	36	10	338	322
(1 0 0)	36	22	458	193
(0 0 1)	37	23	506	162
(0 3 0)	28	10	271	244
(1 1 0)	32	14	319	173
(0 1 1)	35	15	421	173
(0 4 0)	26	8	191	90
(1 2 0)	24	10	209	43
(0 2 1)	33	12	280	141
(2 0 0)	29	9	284	63
(1 0 1)	33	9	321	112
(0 0 2)	32	9	304	35
(0 5 0)	20	6	127	64
(1 3 0)	15	6	129	9
(0 3 1)	29	8	213	72
(2 1 0)	15	8	145	13
(1 1 1)	31	9	271	79
(0 6 0)	17	5	78	39
(0 1 2)	29	12	222	10
(1 4 0)	13	6	95	17
(0 4 1)	25	7	152	80
(0 7 0)	13	3	34	32
(2 2 0)	13	9	111	16
(1 2 1)	22	7	159	64
(0 2 2)	26	9	151	36
(3 0 0)	25	7	186	68
(2 0 1)	32	7	210	58
(1 0 2)	27	6	209	23
(0 0 3)	26	10	209	15
(1 5 0)	10	5	6	11
(0 5 1)	24	6	73	48
(0 8 0)	11	3	7	24
(2 3 0)	14	7	88	16
(1 3 1)	22	7	126	27
(0 3 2)	19	8	104	22
(3 1 0)	22	7	128	33
(2 1 1)	27	7	168	56
(1 6 0)	12	4	5	17
(1 1 2)	16	8	128	13
(0 9 0)	10	4	3	9
(0 1 3)	15	8	131	7
(0 6 1)	19	5	30	33
(2 4 0)	13	4	77	30
(1 4 1)	14	4	88	29
(0 4 2)	16	5	79	9
(3 2 0)	14	6	81	32
(2 2 1)	14	6	94	37
(1 7 0)	10	6	4	6
(4 0 0)	20	6	108	31
(3 0 1)	24	7	120	40
(0 7 1)	11	6	11	7
(0 10 0)	7	6	0	3
(1 2 2)	12	6	80	12
(0 2 3)	14	9	99	6
(2 0 2)	14	7	107	13
(1 0 3)	23	8	137	11
(0 0 4)	22	22	124	2
(2 5 0)	8	6	0	11
(1 5 1)	11	5	35	16
(0 5 2)	10	8	0	7
(1 8 0)	10	6	0	6
(0 8 1)	10	8	0	4
(3 3 0)	10	6	42	18
(2 3 1)	10	4	66	19
(4 1 0)	11	7	74	14

Table 3 (continued)

VBO	J_{max}	J_v	No. validated	No. without validation
(3 1 1)	15	4	92	21
(1 3 2)	9	7	36	1

[a] RRD labels have been determined only for states with J less than 26. VBO=vibrational band origin. J_{max} gives the maximum J value for rovibrational MARVEL states determined on the particular VBO. J_v is the maximum J value for which all labels have been validated.

(b) MARVEL is not able to produce correct labels for assigned transitions; it can only point out inconsistencies within a given dataset.

2.5. Multiphoton transitions

Multiphoton spectra provide valuable information on the energy levels of water extending all the way to dissociation. By use of known intermediate levels and alternative routes to the same upper energy levels, the experiments yield assignment information on the rotational quantum numbers and nuclear spin parity of the upper state.

At present it is not really possible for us to independently validate the energy levels obtained from multiresonance spectra. Standard linelists such as BT2 [194] used here to validate the other levels only extend to about 30 000 cm^{-1}. Although there are a number of *ab initio* computations which study levels, particularly ones with low J, all the way to dissociation [197,201–203], even the most reliable of these [197] does not reproduce the observations near dissociation satisfactorily. Similarly, the near dissociation experiments are difficult and so far have only been successfully performed by one group [35]. For these reasons, the levels obtained by multiresonance spectroscopy are all assessed as being among the energy levels which we deem the least well determined, as seen in Section 3.

Finally, we should also note that while it appears possible to provide meaningful vibrational quantum numbers of the high-lying levels of water probed by the multiresonance experiments, this is generally not true for all levels at high energy [197,204,205]. These experiments particularly probed states of high stretching excitation which appear to keep their localized nature all the way to dissociation. However, it is clear that for many high-lying states neither of the two standard schemes for labeling vibrational levels of water, normal modes or local modes, appear to yield physically reasonable quantum number assignments [197].

2.6. Recalibration

When sets of experimental line positions measured over several decades are combined, systematic differences can be easily identified if several other groups reported high precision values for at least some of the same transitions. Some inconsistencies between studies occur because of mistakes, but others arise simply because the calibration standards changed over time. To correct this situation properly, the best available standards must be applied.

Calibration standards for the infrared were reviewed in 1985 [84], 1992 [207], and in a 1996 IUPAC study [206]. For three decades, the standards involved high-accuracy, Doppler-limited heterodyne frequencies, but only up to 6563.3 cm^{-1}. These were used to obtain positions of easily handled gases, but some lists required correction when better standards appeared [206]. In addition to refined mid-IR standards (*e.g.*, for CO_2 and N_2O at 550–700 cm^{-1} [208] and for CH_4 at 3000 cm^{-1} [209]), new calibration standards now available at near-IR and visible wavelengths enable better scrutiny of the older measurements, especially above 7000 cm^{-1} (see Ref. [210] for atomic potassium and Ref. [211] for $^{127}I_2$ and the references therein).

Data from Fourier transform spectrometers are easily corrected by applying a multiplying factor. For the present study, we relied on one particular laboratory spectrum recorded with the Fourier transform spectrometer at Kitt Peak (FTS-KP) that spanned the 4000 to 14 000 cm^{-1} region using low pressure mixtures of CO, C_2H_2, H_2O, and O_2 (see Ref. [118]). Originally, line centers of the O_2 A-band at 13 100 cm^{-1} were calibrated to precisions of 0.0005 cm^{-1} using CO and C_2H_2 standards near 4250 and 6400 cm^{-1}. However, absolute accuracies were estimated to be only 0.0015($\pm$0.0007) cm^{-1} because the good CO and C_2H_2 positions stopped at 6560 cm^{-1} [118]. Eight years later, Robichaud et al. [212] recalibrated the O_2 positions against two nearby ^{39}K lines [210], and this in turn permitted the earlier mix-gas spectrum [118] to be renormalized based on features of three widely spaced standards (CO, C_2H_2, and O_2). In the present study, line centers of H_2O at 5300, 7400, 8300 and 10600 cm^{-1} (obtained by peak-finding with the apodized spectrum) were compared with collected MARVEL values. Line centers separated by less than 0.05 cm^{-1} from adjacent lines were omitted, as were lines that were too weak ($<15\%$ deep) or too strong ($>90\%$ deep). Table 4 lists near-IR and visible studies identified for correction, along with the multiplicative calibration factors obtained (as was done in Ref. [206]).

During the MARVEL analysis it also became clear that there are other sources of data, obtained by FTS, which might suffer from calibration problems. It is straightforward to determine multiplicative calibration factors with MARVEL [20,22]. The procedure involves the minimization of the root-mean-square (rms) deviation between the

Table 4
Recalibration factors determined during the present study for selected data sources reporting $H_2^{16}O$ transitions. See text for a discussion of the methods used.

Source	Range (cm^{-1})	Calib. factor	Comment
78KaKaKy [70]	33–714	0.999 996 07(7)	MARVEL analysis
95PaHo [105]	177–520	1.0	MARVEL analysis
05HoAnAlPi [138]	212–595	1.0	MARVEL analysis
96PoBuGuZh [107]	407–921	0.999 999 66(2)	MARVEL analysis
82KaJoHo [79]	501–714	0.999 998 84(2)	MARVEL analysis
83Guelachv [81]	1066–2583	0.999 999 77(4)	Previous analysis [20,206]
73CaFlGuAm [62]	2933–4251	0.999 999 93(2)	MARVEL analysis
94Tothb [103]	5750–7988	1.0	FTS, no recalibration needed
80CaFlMa [74]	5934–6400	0.999 999 80(3)	MARVEL analysis
05ToTe [141]	7423–9595	1.0	FTS, no recalibration needed
88MaChFlCa [91]	8057–9482	0.999 999 86(4)	FTS
75FlCaNaCh [66]	8060–9367	1.0	FTS, no recalibration needed
05ToNaZoSh [142]	9250–25 224	1.0	FTS, no recalibration needed
08ToTe [155]	9502–14 495	0.999 999 89(3)	FTS
89ChMaFlCa [92]	9603–11 481	0.999 999 83(3)	FTS
02BrToDu [126]	9676–11 383	0.999 999 90(2)	FTS
99CaJeVaBe [116]	13 185–21 389	0.999 999 96(1)	MARVEL analysis
98PoZoViTe [115]	13 239–15 995	1.0	FTS, no recalibration needed

observed transitions including the source with wavenumbers scaled with a given calibration factor and those produced by MARVEL from the energy levels. The sources identified for recalibration include 73CaFlGuAm [62], 78KaKaKy [70], 80CaFlMa [74], 82KaJoHo [79], 96PoBuGuZh [107], and 99CaJeVaBe [116]. It was found that no recalibration is needed for the following sources containing FTS data: 94Tothb [103], 95PaHo [105], and 05HoAnAlPi [138]. This rms minimization was performed sequentially for all data sources identified as problematic. The multiplicative calibration factors that emerged from these analyses are given in Table 4.

For all the sources identified in Table 4, the experimental data were recalibrated using the calibration factors determined and only the recalibrated transitions were included in the final MARVEL analysis. Recalibrated transitions are distinguished within the dataset by a letter "R" attached to the end of the transition entry.

While there are known calibration problems with some of the ICLAS data [213], during the analysis of ICLAS spectra different calibration lines have been used for every few cm^{-1}. Thus, one cannot determine a unique calibration factor for the whole region covered or employ a constant shift value. Improvement of the ICLAS data via recalibration was thus not attempted here.

2.7. Comments on the data sources

Information on deleted and relabeled transitions given here use MARVEL format; only the new labels are given for the relabeled transitions. All relabeling was performed during the course of the present study.

(2a) 91PeAnHeDe [94]. A hot cell (5 cm in diameter and 1.5 m long, which can be heated up to 1400 K) was employed with a tunable Fourier infrared spectrometer; details are given in Ref. [214]. The typical uncertainty in the determination of the transition frequencies was about 100 kHz (3×10^{-6} cm^{-1}). For the assigned transitions, the maximum value of J (J^{max}) and the maximum value of K_a (K_a^{max}) are 17 and 7, respectively.

(2b) 00ChPePiMa [119]. Coherently generated THz radiation lasers locked to a stabilized etalon, single-pass absorption with a flowing sample. The authors specified one standard deviation for the uncertainties of the lines. The accuracy of the spectrometer was validated by measuring the $4_{2,2}-3_{3,1}$ ground-state transition and comparing it to previous measurements.

(2c) 06GoMaGuKn [145]. Hyperfine structure measurement by the Lamb-dip technique in the millimeter wave and submillimeter wave regions. Frequencies linked to a 10 MHz GPS satellite clock. For the mm-wave absorption spectroscopy the radiation was generated by backward wave oscillators (BWOs). The BWOs were phase stabilized against a 100-GHz RF source, the synthesizers were phase stabilized against a satellite-controlled clock with relative frequency uncertainty of 10^{-9}. InSb bolometer detection at $T=4.2$ K. Second-harmonic detection at 2–5 kHz.

(2d) 87BeKoPoTr [90]. Recorded using a submillimeter-microwave RAD spectrometer; for experimental details see Ref. [215].

(2e) 91AmSc [93]. Spectrum recorded using a millimeter-wave spectrometer; details given in Ref. [216].

(2f) 12YuPeDrMa [164]. Terahertz absorption spectroscopy and far-infrared Fourier-transform emission spectroscopy were employed to measure new rotational and rovibrational transitions and validate some of the lines of existing datasets.

(2g) 83HeMeDe [82]. Frequencies linked to the NIST WWVB radio broadcast time signal. Range of J: 1–10, range of K_a: 1–7. The measurements used mm-wave absorption spectroscopy, RF generators harmonically mixed with 50 GHz Klystron radiation signals phase locked to the WWVB signal. Pressure is not indicated in the paper. Uncertainty in line center determination is dominated by the Doppler width, not by frequency accuracy of the radiation source.

(2h) 81Partridg [78]. The spectra were measured employing a phase modulated NPL-Grubb Parsons Cube interferometer. The spectra were calibrated against at least six H_2O lines measured using a microwave technique. The (J, K_a) ranges are (5–10,0–6) and (1–3,0–1) for the (0 0 0) and (0 1 0) states, respectively. The resolution is up to 0.015 cm^{-1}. Samples of natural water or an enriched mixture with 74% $H_2^{16}O$ were employed. Line positions were measured to a standard deviation of 0.0006 cm^{-1}.

(2i) 95MaOdIwTs [104]. A tunable FIR spectrometer was employed for the measurements. The THz radiation was generated by mixing two CO_2 lasers and microwave radiation. Direct absorption and phase-sensitive detection at 1 kHz. Precision is not indicated in the paper. Line centers were determined to the spectrometer accuracy of 10 kHz, an additional uncertainty of typically 10–20 kHz added in quadrature. Other sources of uncertainty, *e.g.*, signal-to-noise ratio of spectral lines and pressure shifts, were ignored when forming uncertainties. Five high-J lines, $12_{5,7} \leftarrow 12_{4,8}$, $11_{5,7} \leftarrow 10_{6,4}$, $11_{5,6} \leftarrow 10_{6,5}$, $11_{5,7} \leftarrow 11_{4,8}$, and $12_{3,9} \leftarrow 12_{2,10}$ were newly measured. Four lines near 132 cm^{-1}, $5_{5,0} \leftarrow 5_{4,1}$, $6_{5,2} \leftarrow 6_{4,3}$, $7_{5,3} \leftarrow 7_{4,4}$, and $5_{5,1} \leftarrow 5_{4,2}$ reported by 85Johns [86] could not be observed in this study but these lines are confirmed by the present investigation. Following the recommendation of 12YuPeDrMa [164], all uncertainties in this experimental source have been increased to at least 5×10^{-5} cm^{-1}.

(2j) 78KaKaKy [70]. Pure rotational spectrum of H_2O measured by a Michelson-type double beam FTS with 50 cm optical path difference. Pressure (Torr) in the different spectral ranges (cm^{-1}): 30–150: 1.4, 159–390: 1.8, and 390–720: 4.0. The authors quote a maximum resolution of 0.018 cm^{-1} but with the optical path difference it should be more like 0.02 cm^{-1}; in fact, for a number of plots the authors quote 0.03 cm^{-1} resolution. The authors quote accuracies of 0.001 cm^{-1} under favorable conditions. Calibration was done using one line from a He–Ne or Ar ion laser. This assumes a linear scale. The authors also use six H_2O lines from 73FlCa [63], as used by 75ToMa [67], having an accuracy on the order of 0.001 cm^{-1}. Calculated wavenumbers for $H_2^{16}O$ lines use the energies of 73FlCa and at higher J levels the values reported by 73PuRa [64]. For the assigned transitions, $J^{max} = 17$ and $K_a^{max} = 11$. This study was recalibrated to remove systematic differences, see Table 4.

(2k) 04CoPiVeLa [135]. Emission spectra from a RF discharge. The spectra were recorded on an FTS Bruker IFS 120. The wavenumbers were calibrated against data in previous papers. The accuracy of the wavenumbers was originally estimated to be 0.9×10^{-3} cm^{-1}.

(2l) 11DrYuPeGu [162]. The measurements were performed in a water discharge cell using cascaded frequency multiplication, see Ref. [217] for details. Water pressures ranged from < 1.3 hPa (cell evacuated) to 400 hPa for the weakest features. One transition, at 2 527 953.387(200) MHz, a well-known water laser line, was observed in emission.

(2m) 95PaHo [105]. Pure rotational lines with $J^{max} = 17$ and $K_a^{max} = 11$ were measured using a Bruker IFS 120 HR Fourier-transform spectrometer. A White-type cell that gives an absorption path length of 3.2 m was filled with a mixture of $H_2^{16}O$, HD ^{16}O, and $D_2^{16}O$ to a total pressure of 0.50 hPa, and then 0.50 hPa of OCS was added for calibration. The cell, with white polyethylene windows, was at room temperature (295 K). Calibration was carried out using the ν_2 band of OCS with values from Ahonen et al. [218]. The signal-to-noise ratio in the best part of the spectrum was 100 with a spectral resolution of 0.0025 cm^{-1}. The emphasis of the paper was deuterated species and many principal isotopologue lines were in fact saturated.

(2n) 05HoAnAlPi [138]. The emphasis of this paper was to transfer the high accuracy of CO_2 and OCS standards to pure rotational lines of $H_2^{16}O$. FTS study with globar or synchrotron sources. Range of J: 0–17, range of $K_a : 0-11$. Resolution ranging from 1×10^{-3} to 3.5×10^{-3} cm^{-1}. Uncertainties are given for each transition, the range is $10-2000 \times 10^{-6}$ cm^{-1}.

(2o) 97PoZoViTe [168]. Reports laboratory emission spectra recorded with an FTS and reanalysis of sunspot absorption spectrum reported by Wallace et al. [219,220] and initially analyzed by 97PoZoViTea [221].

(2p) 97PoTeBe [167]. Based on data from 96PoBuGuZh [107], which had measurement problems of an unknown origin that made the wavenumber errors higher than expected in a rather erratic fashion. Treatment of these data agrees with those of 96PoBuGuZh [107].

(2q) 96PoBuGuZh [107]. The spectra were recorded on a Bruker IFS 120 HR spectrometer in emission at 1823 K, with a resolution of 0.01 cm^{-1} and a pressure of 20 hPa. A calibration factor of 1.000 048 707 68 was used. The dataset contains transitions up to $J^{max} = 24$ and $K_a^{max} = 23$. This study was recalibrated to remove systematic differences, see Table 4.

(2r) 82KaJoHo [79]. 65 lines corresponding to 71 transitions. Only positions are given. The goal of the paper was to transfer the high accuracy of the ν_1 band of OCS (rms of 3.6×10^{-5} cm^{-1}) to the pure rotational lines of $H_2^{16}O$. Range of J: 6–14, range of $K_a : 1-9$. Resolution of the measurements is 0.0045 cm^{-1}. The precision of the measurements is high, $\pm 4 \times 10^{-5}$ cm^{-1}. This study was recalibrated to remove systematic differences, see Table 4.

(2s) 05CoBeCaCo [174]. Emission spectrum recorded on a Bruker IFS 120 M FTS in an oxyacetylene torch at atmospheric pressure. The calibration used water lines from 02TeBeZoSh [173] checked using a CO standard. The precision of the measurements is 0.02 cm^{-1}. The spectrum was recorded between 500 and 13 000 cm^{-1} but only the low-frequency region was analyzed here; other regions were analyzed in subsequent work [176,177].

(2t) 05ZoShPoTe [175]. This paper deals lines involving highly excited levels of ν_2. Data comes from analysis of the hot emission spectrum recorded by 05CoBeCaCo [174] and the sunspot spectrum originally analyzed by 97PoZoViTeb [222].

(2u) 98EsWaHoRo [170]. The following observed transition was deleted:

1079.2278 0.001 0 2 0 8 1 7 0 1 0 9 4 6 98EsWdaHoRo.00389.

(2v) 06ZoShPoBa [176]. Analysis of the hot emission spectrum recorded by 05CoBeCaCo [174]. 24 transitions have been relabeled.

(2w) 92MaDaCaFl [98]. Pure rotational transitions from air-methane flame spectra.

(2x) 92DaMaCaFlb [97]. The following three observed transitions were deleted:

1200.1726 0.02 0 1 0 21 3 19 0 0 0 22 2 20 92DaMaCaFlb.00056;
1136.0191 0.005 0 1 0 15 8 7 0 0 0 16 9 8 92DaMaCaFlb.00019;
1243.9627 0.005 0 1 0 15 15 0 0 0 0 16 16 1 92DaMaCaFlb.00086.

(2y) 97PoZoTeLo [169]. Laboratory emission spectrum calibrated using 91Toth [95] and sunspot data. The paper concentrates entirely on hot bending transitions and only gives data for transitions of the form $(n+1)v_2 - nv_2$ for $n = 1,2,3$ and 4.

(2z) 99Toth [114]. The following observed transition was deleted:

4147.908200 0.000300 0 0 1 9 4 6 0 0 0 9 0 9 99Toth.03039.

(2aa) 01ByNaSiVo [123]. This paper assigned about 70 lines to states of high bending excitation by considering data from several sources including 86MaChCaFl [88], 89ChMaFlCa [92] and 99CaJeVaBe [116] as well as un-published emission spectra. Five transitions were relabeled.

(2bb) 83Guelachv [81]. 1181 lines of $H_2^{16}O$ were measured in the 1066–2296 cm^{-1} spectral range with an FTS under room temperature conditions and natural abundance. Absorption paths of 16, 24.17, 32.17, and 44.17 m were employed. The maximum uncertainty in the determination of transition frequencies was claimed to be about 1.5 MHz (50×10^{-6} cm^{-1}). The lines were calibrated against CO [223]. Note that the other isotopologue lines from this paper were also recalibrated previously in Parts I and II [20,22] with the well-established calibration factor of 0.999 999 97, see Table 4.

(2cc) 91Toth [95]. The following four observed transitions were deleted:

2148.957000 0.001000 0 1 0 15 6 10 0 0 0 14 5 9 91Toth.00925;
2212.031120 0.000060 0 1 0 14 5 9 0 0 0 13 4 10 91Toth.00953:
1151.0501100 0.05 0 1 0 13 5 9 0 0 0 14 6 8 91Toth.00016;

(2dd) 92DaMaCaFla [96]. The following observed transition was deleted

1568.218800 0.005000 0 4 0 3 3 1 0 3 0 4 2 2 92DaMaCaFla.00136.

(2ee) 93Totha [99]. The following three observed transitions were deleted:

3021.54960000 0.00010000 0 2 0 10 9 1 0 0 0 11 10 2
93Totha.00359;
3046.62350000 0.00010000 0 2 0 9 9 1 0 0 0 10 10 0 93Totha.00378;
3102.174000 0.001000 0 2 0 10 10 0 0 0 0 11 11 1 93Totha.00425.

(2ff) 85BrTo [84]. In the 1100–2200 cm^{-1} region, the positions of the $2v_2$ and v_1 bands of N_2O and the v_2 band of H_2O calibrated previously against the fundamental of CO are readily corrected to achieve absolute accuracies of 0.0001 cm^{-1} or better. The 'precision' was a bit better (about 0.00006 cm^{-1}) for lines well separated from other transitions.

(2gg) 97MiTyKeWi [110]. The spectra were recorded on a FT-IR Bruker IFS 120 HR spectrometer at room temperature with resolution limited by pressure broadening; the pressure-path length product is up to 8700 mbar. The pressure changed between 0.6 and 29.7 mbar. There are OCS and CO_2 lines in the spectrum. The energy levels involved have $J^{max} = 17$ and $K_a^{max} = 11$. The uncertainty of the line position determination is estimated to be about 10^{-4} cm^{-1} or better for good isolated lines and is on average one order of magnitude worse for weaker and overlapping lines.

(2hh) 05Toth [140]. The following observed transition was deleted:

7186.885000 0.003000 0 0 2 9 3 7 0 0 0 10 2 8 05Toth.01870.

(2ii) 73CaFlGuAm [62]. This paper reports lines obtained from FTS measurements of water vapor at low pressure is in the spectral range of 2903–4255 cm^{-1}. A 2 m path difference was used with a home-made FTS. For the principal isotopologue of water, values of line positions were obtained for the v_1, v_3, and $2v_2$ bands as well as the hot band $v_2 + v_3 - v_2$. The precision on wavenumbers relative to each other was estimated to be 0.0005 cm^{-1}, but the absolute accuracy of positions was estimated to be only 0.003 cm^{-1}. This study was recalibrated to remove systematic differences, see Table 4.

(2jj) 73PuRa [64]. The authors used an old grating spectrometer with lower spectral resolution (0.03 cm^{-1}) than the FTS experiments that took over about this time. 73PuRa implemented a "proto-MARVEL" technique to obtain the energy levels. The thesis by Pugh, used in this work, was the source of water-vapor lines in this region (2500–5915 cm^{-1}) in the first HITRAN edition of 1973 [224]. However, a caveat was issued: "the observed contamination of the sample by deuterium to give the HDO abundances varying from 10–200 times normal was not reported." The accuracy of the measurements was estimated to be ± 0.005 cm^{-1}. Seven vibrational bands were treated: (0 0 0), (0 2 0), (1 0 0), (0 0 1), (0 3 0), (1 1 0), and (0 1 1). Naturally, the highest J value was fitted for the ground state and for the asymmetric bend mode, $J^{max} = 15$. The fit was sparse for (0 3 0). Intensity values were also obtained; while the actual number of line intensities measured was probably very large, they are not provided except for wavenumbers of 35 lines that exhibit "intensity anomalies".

(2kk) 02TeBeZoSh [173]. Reports laboratory emission spectra recorded with an FTS and calibrated using 94Tothb [103]. Data were used to analyze a sunspot absorption spectrum reported by Wallace et al. [219,220].

(2ll) 08ZoShOvPo [177]. Analysis of the hot emission spectrum recorded by 05CoBeCaCo [174]. Altogether 140 transitions were relabeled.

(2mm) 09LiNaKaCa [160]. $H_2^{16}O$ lines measured in a highly enriched $H_2^{18}O$ sample (about 10% $H_2^{16}O$ and 90% $H_2^{18}O$).

(2nn) 07MiLeKaCa [152]. Wavenumber calibration was done using HITRAN 2008 [225] water lines. Four water isotopologues were detected. Range of J: 1–20, range of K_a: 1−12. High sensitivity, $\alpha_{min} = 2 \times 10^{-10}$ cm^{-1}. Average uncertainty of the measurements is 0.001 cm^{-1}.

(2oo) 80CaFlMa [74]. The region studied was 5930–6440 cm^{-1}, using an FTS with a resolution of 0.070 cm^{-1}. Positions and intensities for 78 water lines were reported; 31 of them were assigned to the weak third overtone of water, $4v_2$ (with $J^{max} = 10$ and $K_a^{max} = 2$ for this band and $J^{max} = 14$ and $K_a^{max} = 9$ for the $v_2 + v_3$ band). The results of this work were incorporated into HITRAN, although there was some criticism of the work by the late Prof. William Benedict concerning the analysis of the intensities for this band. This study was recalibrated to remove systematic differences, see Table 4.

(2qq) 75ToMa [67]. Measurement in the $1.33-1.45$ μm region using a 1.8 m Jarrel-Ash grating spectrometer. Data are reported for five vibrational states, (0 1 0), (0 2 1), (2 0 0), (0 0 2), and (1 2 0), extracted using the ground-state energies of 73FlCa [63]. FTIR with a resolution of 0.005 cm^{-1} between 2930 and 4255 cm^{-1}. Calibration was done using the super-radiant line of Xe at 2850.6396 cm^{-1}. These lines have uncertainties of 0.001 cm^{-1}. Sample pressure 1–9 mm Hg, path 8–32 m, at $T=295$ K. Calibrations were made with $2v_1 + v_3$ and $v_1 + 2v_2 + v_3$ bands of N_2O by observing the N_2O lines in second order and the H_2O lines in third order of the grating. Further calibration was done by observing the 2.9 μm H_2O lines in first and second order and the 1.4 μm H_2O lines in second and fourth order. Accuracies: 0.007 cm^{-1} for unblended lines, 0.01 and 0.015 cm^{-1} for blended, resolved lines and very weak, observed, and unblended absorptions. The uncertainties are not given for each line and had to be assigned by inspection. Spectral resolution: 0.07 cm^{-1} in the 1.4 μm region. $J^{max} = 15$ and $K_a^{max} = 7$.

(2rr) 11MiKaWaCa [163]. Based on an absorption spectrum recorded using water at natural isotopic abundance.

(2ss) 05ToTe [141]. Minimum error set at 0.001 cm^{-1}. No calibration procedure is discussed. The energies are in "good agreement" with energy levels determined by 04MaRoMiNa [136], who studied a neighboring region. The following line was relabeled:

8752.42358 0.001831 0 3 1 11 8 4 0 0 0 11 8 3 05ToTe.2646.

(2tt) 88MaChFlCa [91]. The authors used the Kitt Peak FTIR to measure water vapor spectra in the 7900–9500 cm^{-1} region. The measurements were made at 300 K under the following conditions:

Sample	Resolution/ (cm^{-1})	P (atm)	Path length (cm)	%$H_2^{16}O$
Natural	0.0174	22.8×10^{-3}	43 396	0.997
Natural	0.0145	1.97×10^{-3}	43 396	0.997
^{18}O enriched	0.0112	3.68×10^{-3}	21 742	0.27
^{18}O enriched	0.0112	3.68×10^{-3}	4900	0.27
^{18}O enriched	0.0112	0.96×10^{-3}	2494	0.27
^{17}O enriched	0.0112	6.18×10^{-3}	21 742	0.79

It appears that some of these spectra are the same as those used in 86MaChCaFl [88]. However, for ^{18}O and ^{17}O the resolution given above is different. S/N was between 500 and 2300. There is no discussion about the frequency calibration of the spectra. 441 rotational levels with $J^{max} = 14$ and $K_a^{max} = 8$ are reported. For each energy state, the tables report the uncertainty as 1 standard deviation but systematic error is not accounted for.

(2uu) 75FlCaNaCh [66]. Grating spectrometer spectra, calibrated against CO lines. Two methods were employed to probe near-IR rovibrational spectra. First, room temperature spectra on the strongest lines were acquired with a 10 m focal length grating spectrometer, pathlength of 100 m, $p=7$ Torr, Carbon rod light source, PMT detection. Second, higher-temperature (60 °C) spectra were acquired with a Fourier transform spectrometer. Pathlength of 40 m, $p=90$ Torr. Near-IR line positions measured by the two methods agree to within the 0.005 cm^{-1} measurement uncertainty. Only a single uncertainty reported (no transition-dependent values). Range of J values: 1–13, range of $K_a : 0-8$. The following two measured lines were relabeled:

8436.59100 0.005000 1 1 1 14 1 14 0 0 0 15 1 15 75FlCaNaCh.00228;
8892.06880 0.020001 1 1 1 10 3 7 0 0 0 10 3 8 75FlCaNaCh.00862.

(2vv) 05ToNaZoSh [142]. Spectra were recorded in a Bruker IFS 120M spectrometer and calibrated using the I_2 visible spectrum. The resolution is 0.03–0.06 cm^{-1}. The calibrated line positions were shown to agree with previous studies and with HITRAN to better than 5×10^{-4} cm^{-1}. 422 lines were relabeled.

(2ww) 08ToTe [155]. These authors undertook a comprehensive reanalysis of the FTS data of 02ScLeCaBr [128], some of whose results were reported by 02ToTeBrCa [130], who only reported long pathlength data. 08ToTe results involved a simultaneous fit to data reported at several path lengths. The fitting method employed constrained the line positions of transitions with the same upper energy levels. The results were calibrated using HITRAN (i.e., 02BrToDu [126], 03MeJeHeVa [131], and 02CoFaCaCl [129]). 60 lines have been relabeled. This study was recalibrated to remove systematic differences, see Table 4.

(2xx) 03NaCa [132]. 6 lines were relabeled.

(2yy) 89ChMaFlCa [92]. 14 lines were relabeled. This study was recalibrated to remove systematic differences, see Table 4.

(2zz) 02BrToDu [126]. Calibrated 2–0 and 3–0 bands of CO at 2.3 and 1.5 μm and checked with 89ChMaFlCa [92] and 94Totha [102]; the precisions of the line positions was found to be ± 0.0003 cm^{-1}. 21 lines were relabeled. This study was recalibrated to remove systematic differences, see Table 4.

(2aaa) 09GrBoRiMa [34]. This paper reports three-photon spectra of $H_2^{16}O$ and thus probes energy levels close to the dissociation limit of water. Only data on transitions involving the third photon, which is in the frequency range 10 305–14 619 cm^{-1}, were included since the lower-lying energy levels are better determined from higher resolution spectra. The addition of the following three extra double-resonance lines (O.V. Boyarkin and N.F. Zobov, private communication, 2012) not reported in 08GrMaZoSh [33] was necessary to connect the data:

11 174.40 0.003000 8 0 0 4 1 4 3 0 1 5 1 5 Boyarkin.1;
11 290.38 0.003000 8 0 0 1 1 0 3 0 1 1 1 1 Boyarkin.2;
11 332.73 0.003000 7 0 1 6 1 5 3 0 1 6 0 8 Boyarkin.3.

(2bbb) 06MaNaKaBy [147]. 38 lines were relabeled.
(2ccc) 97FlCaByNaa [111]. 28 lines were relabeled.

(2ddd) 94Totha [102]. Five lines were relabeled.

(2eee) 02ToTeBrCa [130]. A theoretical analysis of data reported by 02ScLeCaBr [128]. These data were subsequently included in a larger reanalysis by 08ToTe [155].

(2fff) 08CaMiLi [157]. 30 lines were relabeled.

(2ggg) 99CaJeVaBe [116]. Calibration was performed with the I_2 line positions with the values of Gerstenkorn and Luc [226]. The raw spectra were shifted by $+0.002\,353\,\mathrm{cm}^{-1}$, corrected for the refractive index of air (the spectrometer was not evacuated), and then multiplied by a factor of 1.000 001 78. No known problems with the lines, although a small, further overall calibration factor may be needed if the I_2 calibration described in the paper was not quite right. 494 lines were relabeled and 20 deleted. This study was recalibrated to remove systematic differences, see Table 4.

(2hhh) 98PoZoViTe [115]. Theoretical analysis of measurement is taken from Mandin et al. [87] who used an FTS built by Brault. Originally, the uncertainty in line positions was estimated to vary between 0.002 to $0.015\,\mathrm{cm}^{-1}$. 110 lines were relabeled.

(2iii) 05KaMaNaCa [143]. The goal of this paper was the detection of very weak lines in a region where atmospheric detection of water dimer was claimed. I_2 lines were used as references for the calibration. Range of J: 2–15, range of K_a: $0-8$. No uncertainty values are given in the paper for the lines. High sensitivity, $\alpha_{min} = 3 \times 10^{-10}\,\mathrm{cm}^{-1}$. Five lines were relabeled.

(2jjj) 08GrMaZoSh [33]. This paper reports two photon spectra of $H_2^{16}O$ performed under conditions whereby the water can collisionally relax between the first and second photon absorption. The work also contains lines measured by 07MaMuZoSh [32] who did not allow for collisional relaxation. Both works probe energy levels between 26 000 and $34\,200\,\mathrm{cm}^{-1}$. Only data on transitions involving the second photon, which is in the frequency range 13 531–$17\,448\,\mathrm{cm}^{-1}$, were included since the route to the final state involves a non-radiative process.

(2kkk) 11BeMiCa [161] Four lines were relabeled.

(2lll) 85CaFlMaCh [85]. FTIR measurements at Kitt Peak Solar Observatory and a grating and a Bomem FT with a 33 m path. Measurement conditions were as follows:

Range	Resolution (cm^{-1})	P (Torr)
9000–14 500	0.017	1.5
9000–14 500	0.017	17.4
12 000–16 500	0.013	1.5
12 000–16 500	0.013	17.3
15 500–21 000	0.019	17.1
18 000–19 500	0.025	17.6
18 000–23 000	0.028	17.1
21 050–21 400	0.040	17.8
22 350–22 700	0.040	18.4.

The signal to noise ratio was greater than 500:1. Part of the atmospheric path is in the laboratory so the path area was purged with dry N_2 to reduce the effect of water lines in the lab. Resolution is $23-40 \times 10^{-3}\,\mathrm{cm}^{-1}$, spectra measured in Ottawa had $0.04\,\mathrm{cm}^{-1}$ unapodized resolution. Calibration for the wavenumber scale was a problem, solved by recording spectra in regions. The first spectrum was recorded between 4000 and $9000\,\mathrm{cm}^{-1}$ with N_2O present as the calibration standard. Higher wavenumber spectra had overlap with the lower so that lines present in two spectra

allowed the upper wavenumber spectra to be calibrated. Estimated errors in line position was $2 \times 10^{-3}\,\mathrm{cm}^{-1}$ for intense well-isolated lines down to $25 \times 10^{-3}\,\mathrm{cm}^{-1}$ for the weakest lines. The authors measured 1174 line positions from which 539 vibrational–rotational energies were deduced. $J^{max} = 11$ and $K_a^{max} = 7$. For each energy state, the tables report the uncertainty as 1 standard deviation. There is no accounting for systematic error in the experimental uncertainties. The following three lines were relabeled:

8436.591 0.005 1 1 1 14 1 14 0 0 0 15 1 15 75FlCaNaCh.00228;
8818.7746 0.005 2 1 0 8 3 5 0 0 0 8 2 6 75FlCaNaCh.00745;
8892.0688 0.020 1 1 1 10 3 7 0 0 0 10 3 8 75FlCaNaCh.00862

(2mmm) 00ZoBePoTe [120]. This paper presents an analysis of the high-frequency data originally measured with a Bruker IFS 120 M FTS by 99CaJeVaBe [116] and uses the same calibration procedure. The original estimated uncertainty in the line positions is $0.004\,\mathrm{cm}^{-1}$. However, during the MARVEL analysis this proved to be too optimistic and had to be increased.

(2nnn) 05DuGhZoTo [144]. There are 43 reported transitions extending into the near ultraviolet; this is the highest frequency one-photon vibration-rotation spectrum of water available. No information is given about calibration.

2.8. Variational validation

As an independent validation of the experimental transition wavenumbers and the derived MARVEL energy levels and their labels, systematic and mostly automated comparisons were made with the results of state-of-the-art variational nuclear motion computations. For this comparison, the so-called BT2 linelist [194] was principally used; this linelist was computed using a spectroscopically determined PES [43], an *ab initio* DMS [47], and the DVR3D [227] nuclear motion program suite.

Those measured transitions involving a MARVEL energy level which did not have a matching variational counterpart within $1.0\,\mathrm{cm}^{-1}$, with proper rotational parity (Table 1), were investigated individually and the MARVEL process was repeated until all MARVEL levels had variational counterparts within the chosen cut-off value. There were only a couple of cases where the deviation between the BT2 and MARVEL energy levels was larger than $1.0\,\mathrm{cm}^{-1}$. For transitions removed at this stage, see the appropriate comments in Section 2.7 and the supplementary data.

Any MARVEL rotational–vibrational energy level obtained as part of this work which differed by more than $0.5\,\mathrm{cm}^{-1}$ from its variational counterpart was subject to further scrutiny. When variational results are used for validation, we can rely on a well-known feature of such calculations: the smooth and slow variation of obs − calc residuals for the energy levels of a particular vibrational state having the same K_a and increasing J values [228]. The longest obs − calc sequences could be investigated for the hot spectra, where transitions involving J as high as 42 have been detected. The obs − calc residues for levels with a given K_a but different K_c diverge as J increases, hindering the assignment of the dense observed spectrum without detailed

consideration of near degeneracies. The obs − calc trends for the highly excited vibrational states are not particularly smooth as they can be strongly perturbed by nearby states. Cases with erratic obs − calc trends were additionally checked to see whether the calculated energy level set includes the resonance partner, whose energy level has to be close to the level under investigation and whose quantum numbers should satisfy the conventional Coriolis-, Fermi-, or Darling–Dennison-type resonance interaction rules, or some combination of them. Where necessary, labels were changed assuming similar increases in rotational energies as a function of J and K_a for similar vibrational states with the same v_2 quantum number as well as quasi-degeneracy of rotational levels with K_a close to J or K_a equal to 0 or 1.

At the end of a MARVEL analysis cycle, the MARVEL energy levels obtained were distributed into bins having different J values and parities (thus we used only exact quantum numbers for the matching). These bins were checked against ones derived variationally from the best possible PES [46], which was also refined during this study taking into account the best MARVEL energy levels up to $J=15$. For each J up to $J=15$, MARVEL energy levels which deviated by more than 3σ from their variational counterparts were checked individually. Transitions which proved to be inconsistent with this type of information were removed or their uncertainties were adjusted to reflect the knowledge gained. As the results of Table 5 show, at the end all MARVEL energy levels up to $J=15$ are reproduced by the variational energy levels with an accuracy better than $0.05\,\mathrm{cm}^{-1}$. Of course, as J increases the average deviation between the variational and the MARVEL levels grows. The success of these comparisons reflect simultaneously the high quality of the PES employed for the nuclear motion computations and of the MARVEL energy levels derived.

2.9. Post-MARVEL validation

For a number of transitions which proved to be outliers by combination difference relations, the experimental uncertainties were increased manually (see Section 2.7). This extra validation and the subsequent adjustment were done when the energy of an upper rotational–vibrational state deviated far more from the corresponding mean value established by the lower MARVEL energy levels plus the transition wavenumbers than the stated experimental uncertainty. Using the MARVEL protocol can result in similar adjustments automatically if the error associated with a transition is an outlier and all the data have similar accuracy. However, a problem arises if an erroneously small experimental uncertainty is attached to what is actually a much less accurate experimental datum, the same level is involved in several measurements, and other transitions in the combination difference relations, though consistent, have formally much larger uncertainties. In this case the MARVEL energy level will be determined by the formally most accurate transition which, in fact, represents an outlier. We attempted to check carefully all such cases but it is extremely hard to ensure that all problematic cases were properly identified and treated.

At this stage we also checked whether the rovibrational MARVEL energy lies below the corresponding vibrational band origin (VBO). If this happened, the corresponding labeling was investigated and adjusted to comply with the majority of the data. At the end of this process we were left with a list of 182 156 (68 027 para and 114 129 ortho) validated transitions. The 2511 transitions deleted from the initial list may be incorrectly measured or assigned; however, they may also be correct but have a large uncertainty and are thus dropped when higher accuracy data are available from other measurements. In the end only 60 transitions proved to be orphans or part of FSNs.

3. MARVEL energy levels

Table 6 contains MARVEL vibrational band origins (VBO) for $H_2{}^{16}O$. For each VBO, Table 6 also gives the number of rovibrational energy levels validated within this work and based on the original 184 667 transitions. From these transitions we derive a final set of 18 486 energy levels. One can observe that, due to the large number of measured transitions, the list of VBOs of the main isotopologue is much more complete than in Parts I and II for the minor isotopologues of water. If a polyad number $P=2v_1+v_2+2v_3$ is defined, all VBOs are determined experimentally up to $P=5$. The first three missing VBOs are $(1\,4\,0)$, $(0\,7\,0)$, and $(1\,5\,0)$ at about $10\,000\,\mathrm{cm}^{-1}$; otherwise the coverage is complete up to $P=7$. There are eight measured VBOs out of 10 for $P=7$. There are very few VBOs below about $18\,000\,\mathrm{cm}^{-1}$ for which rotational–vibrational levels have not been determined at all. The first VBO is $(0\,0\,5)$ (the highest-lying $P=10$ VBO) which has no measured and assigned rovibrational levels. For $P=11$ and beyond there are more and more VBOs which have no measured rovibrational lines.

A comparison can be made between the original set of observed transitions and those calculated from the "experimental" energy levels determined by MARVEL; this is presented in Fig. 1. About 36.0% and 83.7% of all transitions are reproduced within 0.001 and $0.01\,\mathrm{cm}^{-1}$, respectively.

A comparison of the experimental (MARVEL) and variational (BT2 [194]) energy-level values is given in Fig. 2. Clear trends are visible in Fig. 2 showing the systematic nature of the errors of most of the computed rotational–vibrational transitions.

The set of MARVEL energy levels derived from processing the validated observed transitions can be used to predict a large number of rovibrational transitions often with positions at a level of experimental accuracy. These line positions were augmented with variational, one-photon absorption intensities corresponding to $T=296\,\mathrm{K}$ and obtained from BT2 [194]. The resulting list can be considered as one of the key results of the present investigation. The total number of predicted transitions with intensities larger than 1.0×10^{-28} and 1.0×10^{-32} cm molecule^{-1} is 66 582 and 211 489, respectively. Observed, MARVEL predicted, and variational $H_2{}^{16}O$ transitions are shown in the panels of Fig. 3. This figure is especially important for future experimental studies of

Table 5

Standard deviation, in cm^{-1}, of the $H_2^{16}O$ MARVEL energy levels with respect to energies obtained from variational nuclear motion computations executed with a PES based on Ref. [46] and improved as part of this study and an exact kinetic energy operator.

J	No. of levels	Standard deviation
0	78	0.0234
1	270	0.0220
2	475	0.0315
3	673	0.0294
4	842	0.0334
5	997	0.0313
6	1069	0.0323
7	1104	0.0351
8	1037	0.0369
9	950	0.0385
10	851	0.0439
11	752	0.0535
12	672	0.0632
13	605	0.0693
14	560	0.0750
15	519	0.0822
All	11 454	0.0462

the high-resolution spectra of $H_2^{16}O$. It is important to point out that in the low end of the spectrum, below about $10\,000\ cm^{-1}$, there is a huge number of "observed" lines with predicted intensities down to $1 \times 10^{-30}\ cm\ molecule^{-1}$. Such a complete coverage by the "observed" transitions is due to the existence of a large number of energy levels derived from the analysis of hot emission spectra, and these transitions have never been measured directly in absorption.

The accuracy and precision of the MARVEL energy levels determined in this study depend upon quite a large number of factors. Perhaps most important among these is the accuracy of the measured transitions. Experimental uncertainties provided in the original sources are often overly optimistic, by an order of magnitude for some of the lines (weak, blended, etc.). Consequently, in a large number of cases the published uncertainties had to be increased substantially during the course of the MARVEL analyses, either before or during the robust reweighting procedure. Since our analyses attempted to utilize all the experimental information available for the Task Group in the form of results published in scientific journals, there are many energy levels which are involved in multiple transitions measured by several experimental groups utilizing different spectrometers, different setups, and different experimental conditions. We consider an energy level particularly well determined, *i.e.*, accurate and precise, if it is involved in more than 12 transitions and there are at least five independent experimental investigations which determined this energy level. These energy levels are graded as A^+, see supplementary data. This means that the value of the energy level, within the stated uncertainty, and the label of the energy level are completely dependable. These energy levels should be particularly useful for future studies and in modeling work. Energy levels which are involved in more than 10 transitions and are also part of transitions published in at least four independent experimental investigations are graded

as A^-. These energy levels and their labels should still be considered dependable. Energy levels which are involved in at least eight transitions and are also part of transitions published in at least three independent experimental investigations are graded as B^+. Energy levels which are involved in at least six transitions and are also part of transitions published in at least two independent experimental investigations are graded as B^-. All other energy levels are graded as C. This means that there are energy levels with the worst grade, C, which may be accurately known. Nevertheless, it is expected that since many of the grade C energy levels come from a single source, their uncertainty may not be dependable. Our recommendation for transitions is that they should be graded using the grade of the lower graded energy level involved.

3.1. Status of highly accurate transitions

The agreement between the MARVEL predicted and the experimental pure rotational transitions improved slightly by the recalibration of the experimental transitions. Another source of inaccuracy when combining measured line positions from several sources is due to pressure effects, not corrected for in this study. In order to measure the weakest spectral features in several experiments the pressure had to be increased beyond 20 hPa (for details, see Table 2). Analysis of some of the experiments have also used different line profiles and line profile parameters. This could result in small shifts in the line centers. Furthermore, since both the ortho and para components of the SN of $H_2^{16}O$ contain an extremely large number of cycles of widely varying size, even the inclusion of a few seemingly inconsequential transitions with incorrect uncertainties can distort the value and the uncertainty of MARVEL energy levels which would be determined accurately and precisely by a subset of the experiments. The effect of all these factors is reflected in MARVEL uncertainties larger than otherwise expected for several "highly accurate" rotational–vibrational levels (see Figs. 4 and 5).

The MARVEL uncertainties of the pure rotational levels are uniformly larger, perhaps by an order of magnitude, than is usual for lines coming from microwave determinations. To show that this is due to the (inappropriate) uncertainties of the upper states we performed a MARVEL analysis of the pure rotational states. MARVEL can reproduce the microwave uncertainties very nicely, down to the level of the experimental uncertainties, as also observed before [26].

As seen in Table 7, MARVEL can reproduce recent accurate THz measurements [162] rather well, usually better than the stated uncertainty of the MARVEL transitions would suggest. This is a pleasing result as the energy levels participating in the THz transitions are involved in a large number of other transitions of lower accuracy which could distort their prediction. Nevertheless, for many observed transitions in the THz region the difference between the MARVEL and the 11DrYuPeGu [162] transitions is outside the original experimental uncertainty limits. Reproduction of other measurements [104,135,146] of the same transitions is also excellent as the data collected in Table 7 demonstrate.

Table 6
MARVEL vibrational band origins (VBO) for $H_2^{16}O$, with normal-mode ($v_1v_2v_3$) labels, MARVEL uncertainties, and the number of validated rotational–vibrational levels (RL) associated with the vibrational levels in the present database.[a]

P	$v_1v_2v_3$	VBO/cm^{-1}	Unc.[a]	RL
0	0 0 0	0.000000[b]	0	1171
1	0 1 0	1594.746292	20	1063
2	0 2 0	3151.629847	190	819
	1 0 0	3657.053251	200	820
	0 0 1	3755.928548	18	867
3	0 3 0	4666.790461	493	523
	1 1 0	5234.975555	324	517
	0 1 1	5331.267252	159	680
4	0 4 0	6134.015008	218	290
	1 2 0	6775.093505	238	255
	0 2 1	6871.520195	243	451
	2 0 0	7201.539855	437	359
	1 0 1	7249.816921	842	472
	0 0 2	7445.056211	10 001	374
5	0 5 0	7542.372492	5000	191
	1 3 0	8273.975692	309	139
	0 3 1	8373.851351	325	294
	2 1 0	8761.581578	266	160
	1 1 1	8806.998969	167	367
	0 1 2	9000.136035	430	238
6	0 6 0	8869.950054	5000	119
	1 4 0	[9724.3]		114
	0 4 1	9833.582928	237	232
	2 2 0	10 284.364368	345	127
	1 2 1	10 328.729259	160	226
	0 2 2	10 521.757715	513	188
	3 0 0	10 599.685969	219	254
	2 0 1	10 613.356302	365	281
	1 0 2	10 868.874717	250	238
	0 0 3	11 032.404120	227	226
7	0 7 0	[10 086.1]		68
	1 5 0			19
	0 5 1	11 242.775681	764	122
	2 3 0	11 767.388973	657	103
	1 3 1	11 813.206888	141	154
	0 3 2	12 007.774346	476	128
	3 1 0	12 139.315308	347	160
	2 1 1	12 151.253943	191	228
	1 1 2	12 407.662025	200	140
	0 1 3	12 565.006418	154	138
8	0 8 0	11 253.997325	22 000	39
	1 6 0			22
	0 6 1	[12 586.0]		64
	2 4 0	[13 205.1]		107
	1 4 1	13 256.155010	6205	118
	0 4 2	[13 453.7]		89
	3 2 0	13 640.716557	5000	113
	2 2 1	13 652.653219	324	130
	1 2 2	13 910.893586	744	93
	0 2 3	14 066.193560	234	107
	4 0 0	13 828.274703	426	142
	3 0 1	13 830.936841	343	161
	2 0 2	14 221.158521	448	120
	1 0 3	14 318.812128	333	148
	0 0 4	14 537.504321	1000	126
9	0 9 0			14
	1 7 0	[13 661.0]		10
	0 7 1	13 835.372240	354	18
	2 5 0			11
	1 5 1	14 647.973320	3917	52
	0 5 2			7
	3 3 0			62
	2 3 1	15 119.028730	651	85
	1 3 2			37
	0 3 3	15 534.708852	600	72
	4 1 0	15 344.502805	897	88
	3 1 1	15 347.956812	654	114

Table 6 (continued)

P	$\nu_1\nu_2\nu_3$	VBO/cm^{-1}	Unc.[a]	RL
	2 1 2	15 742.797275	2350	72
	1 1 3	15 832.765391	565	96
	0 1 4			5
10	0 10 0			3
	1 8 0			7
	0 8 1			4
	2 6 0	[15 871]		6
	1 6 1	[15 969]		7
	0 6 2	[16 215]		8
	3 4 0	[16 534.5]		49
	2 4 1	16 546.318552	1000	53
	1 4 2	[16 795.9]		65
	0 4 3	[16 967.6]		20
	4 2 0	16 823.318521	1000	73
	3 2 1	16 821.631065	4140	81
	2 2 2	17 227.379521	1000	53
	1 2 3	17 312.551252	1000	73
	0 2 4	[17 526.3]		6
	5 0 0			70
	4 0 1	16 898.842178	2609	90
	3 0 2	17 458.213241	551	74
	2 0 3	17 495.527952	1000	100
	1 0 4	17 748.106721	1000	50
	0 0 5			0
11	*0 11 0*			0
	1 9 0			3
	0 9 1			3
	2 7 0			6
	1 7 1			2
	0 7 2			2
	3 5 0			11
	2 5 1			8
	1 5 2			12
	0 5 3			22
	4 3 0			51
	3 3 1	18 265.821152	1000	61
	2 3 2			2
	1 3 3	18 758.635911	4444	44
	0 3 4			12
	5 1 0	18 392.777521	1000	60
	4 1 1	18 393.314552	1000	59
	3 1 2			11
	2 1 3	18 989.959852	1000	52
	1 1 4			3
	0 1 5			4
12	0 12 0			2
	1 10 0			0
	0 10 1			2
	2 8 0			2
	1 8 1			2
	0 8 2			4
	3 6 0	[19 223.5]		7
	2 6 1	[19 250]		7
	1 6 2			0
	0 6 3	[19 720.2]		9
	4 4 0	[19 677.8]		34
	3 4 1	19 679.192452	1000	44
	2 4 2			0
	1 4 3			3
	0 4 4			14
	5 2 0	[19 864.7]		24
	4 2 1	19 865.284652	1000	20
	3 2 2			11
	2 2 3	20 442.777352	1000	31
	1 2 4			0
	0 2 5			0
	6 0 0	19 781.322742	577	73
	5 0 1	19 781.102852	1000	73
	4 0 2	[20 534.5]		38
	3 0 3	20 543.128552	1000	41

Table 6 (*continued*)

P	$\nu_1\nu_2\nu_3$	VBO/cm^{-1}	Unc.[a]	RL
	2 0 4			0
	1 0 5			3
	0 0 6			0
13	0 13 0			3
	2 9 0			1
	0 9 2			2
	3 7 0			2
	2 7 1			5
	0 7 3			2
	4 5 0	[21 052]		11
	3 5 1	[21 053]		10
	5 3 0	[21 312]		16
	4 3 1	21 314.448152	1000	22
	3 3 2			2
	2 3 3	[21 867]		3
	1 3 4			1
	0 3 5			1
	6 1 0			43
	5 1 1	21 221.827252	1000	41
	4 1 2			1
	3 1 3	[22 015]		8
	2 1 4			2
	1 1 5	[22 508]		31
14	3 8 0			1
	4 6 0	[22 376]		7
	3 6 1	[22 377]		4
	4 4 1			1
	6 2 0	[22 626]		5
	5 2 1	[22 629]		6
	4 2 2			4
	1 2 5	[23 934]		9
	7 0 0	22 529.295101	979	63
	6 0 1	22 529.440683	639	49
	5 0 2	[23 401]		0
	4 0 3	[23 405.4]		7
15	4 7 0			1
	4 5 1			1
	7 1 0	[23 942]		7
	6 1 1	[23 947]		9
16	8 0 0	[25 120]		45
	7 0 1	25 120.277883	639	44
	6 0 2			2
	5 0 3			2
17	5 3 2	27 502.659624	20 000	17
	4 3 3			8
	6 1 2	27 574.909624	20 000	15
	5 1 3			6
18	6 2 2			5
	5 2 3			4
	9 0 0	27 540.689624	20 000	18
	8 0 1			18
19	9 1 0	28 934.139624	20 000	5
	8 1 1			3
20	10 0 0	29 810.849624	20 000	29
	9 0 1			27
	8 0 2	31 071.569624	20 000	7
	7 0 3			5
21	10 1 0	31 207.089624	20 000	7
	9 1 1			3
22	11 0 0	31 909.678623	20 000	12
	10 0 1			9
23	11 1 0	33 144.708623	20 000	11
	10 1 1			10
24	4 6 5			1
	12 0 0	33 835.248623	20 000	12
	11 0 1	33 835.222129	20 000	12
	10 0 2			7
	9 0 3	35 509.676937	20 000	8
25	11 3 0			3
	10 3 1			5

Table 6 (*continued*)

P	$v_1 v_2 v_3$	VBO/cm^{-1}	Unc.[a]	RL
	10 1 2	36 740.597407	20 000	4
	9 1 3	36739.776937	20 000	5
	8 1 4			2
	7 1 5			1
26	12 2 0	36 179.317409	20 000	6
	11 2 1			6
	13 0 0	35 585.957409	20 000	13
	12 0 1	35 586.006937	20 000	13
27	13 3 1	40 262.001364	20 000	1
	12 3 0	37 311.277407	20 000	5
	11 3 1	37 309.846937	20 000	5
	13 1 0	36 684.047409	20 000	9
	12 1 1	36 684.876937	20 000	7
28	13 2 0	37 765.647409	20 000	5
	12 2 1			5
	14 0 0	37 122.697409	20 000	15
	13 0 1	37 122.716937	20 000	16
	11 0 3			1
29	14 1 0	38 153.247409	20 000	8
	13 1 1	38 153.306937	20 000	10
	12 1 2	40 044.566912	20 000	5
	11 1 3	40 044.671147	20 000	8
30	14 2 0	39 123.767409	20 000	11
	13 2 1			8
	15 0 0	38 462.517407	20 000	12
	14 0 1	38 462.536937	20 000	14
	13 0 2			3
	12 0 3	40 704.156147	20 000	3
31	13 3 1	40 262.001147	20 000	1
	15 1 0	39 390.257409	20 000	13
	14 1 1	39 390.216937	20 000	14
32	15 2 0			10
	14 2 1	40 226.261147	20 000	12
	16 0 0	39 574.547409	20 000	12
	15 0 1	39 574.536937	20 000	15
33	16 1 0	40 370.546912	20 000	8
	15 1 1	40 370.781147	20 000	8
34	16 2 0			1
	15 2 1	41 121.606147	20 000	2
	17 0 0	40 437.226912	20 000	12
	16 0 1	40 437.211364	20 000	12
35	17 1 0	40 984.636911	20 000	5
	16 1 1			5
36	18 0 0	40 947.486911	20 000	5
	17 0 1	40 945.693147	20 000	6
37	19 0 0	41 101.336912	20 000	5
	18 0 1	41 100.053364	20 000	6

[a] The VBOs are reported in the order of the polyad number P defined as $P = 2v_1 + v_2 + 2v_3$. All the VBOs are listed up to $P = 12$ but only selected ones holding measured rovibrational states beyond it. The uncertainties (Unc.) are given in units of 10^{-6} cm^{-1}. For VBOs not determined by the available experimental data, approximate computed VBOs, based on $J > 0$ rotational levels as reported in Ref. [36], are given in brackets. These values should only be used for guidance about the VBOs, although their accuracy is expected to be better than 0.1 cm^{-1}. No uncertainties are given for these VBOs. For completeness, some of the lower-P VBOs which are involved in none of the observed rovibrational transitions are also given. The corresponding labels are printed in italics for guidance. The VBOs are ordered according to their formal labels within a given P, which corresponds to their energy order up to $P = 23$ and thus they appear in increasing energy order.

[b] The value of the vibrational ground state was fixed to zero with zero uncertainty.

3.2. Comparison with previous sets of energy levels

There are several labeled energy-level lists available for $H_2{}^{16}O$. Those which were available to us in an electronic form were used for a comparison with MARVEL energy levels. Note that no attempt was made to relabel the energy levels of the original sources. This means that in a number of cases where the present study relabeled the transitions a discrepancy is kept between the two data sources. For example, most of the more than 500 mismatches between the MARVEL and Ref. [28] energy levels are due to this.
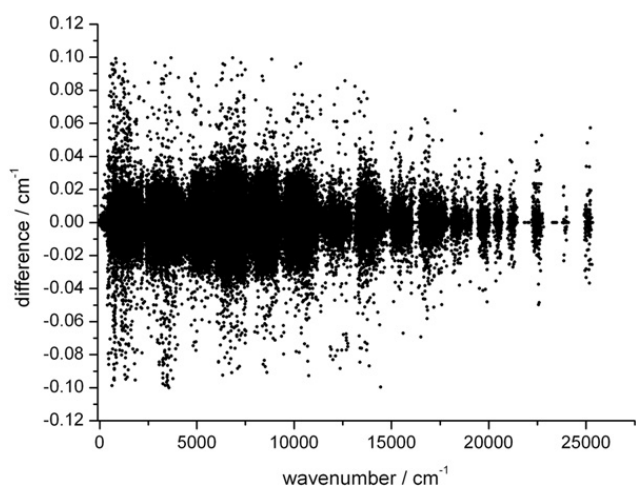
Fig. 1. Differences between MARVEL-based and measured transition wavenumbers for $H_2^{16}O$.
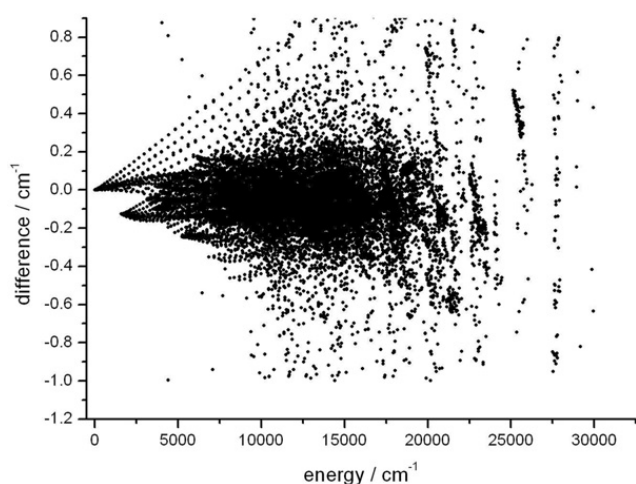
Fig. 2. Differences between the present MARVEL energy levels and their counterparts present in the BT2 linelist [194].


Fig. 3. Comparison of intensities at 296 K for one-photon absorption transitions of $H_2^{16}O$ up to 30 000 cm^{-1}. Top panel—measured lines; second panel—MARVEL predicted but omitting the above observed line; third panel—sum of the first two; and bottom panel—all lines predicted by variational computations (BT2 [194]). The weakest measured intensities come from emission spectra of hot water which are difficult to obtain directly in absorption.

One of the most accurate effective-Hamiltonian-based energy-level lists available for $H_2^{16}O$ is published in Ref. [135]. The eight panels of Fig. 6 present a comparison between the accurate, EH-based energy levels of Ref. [135] and their MARVEL counterparts for the first eight VBOs of $H_2^{16}O$. The agreement is outstanding for (0 0 0): there is no deviation larger than 0.005 cm^{-1}. The agreement is somewhat less perfect for a few rovibrational levels of the excited vibrational states. Nevertheless, no systematic deviations can be observed. It is possible that the energy levels of Ref. [135] are still more accurate than the present MARVEL levels but this would require further studies based on a new and larger set of available experimental results to derive new parameters for the effective Hamiltonian and the inclusion of extensive, more accurate new measurements into the MARVEL analysis.

Comparison between the present MARVEL energy levels and those of a previous large set of "measured" energy levels compiled in Ref. [28] are shown in Fig. 7. The agreement is excellent up to about 5000 cm^{-1}. Beyond this, the scatter is considerably larger but still lower than the accuracy of many of the underlying rovibrational transitions.

Further figures which are given in the supplementary data show the agreement between the present MARVEL and the literature energy levels [127,130,132,135–137, 141,143,144,147,163,174–176] is excellent in almost all cases. There are a number of problematic energy levels, which we are not able to reproduce within 0.04 cm^{-1}. In nearly all cases these differences are caused by changes in labeling used to describe particular energy levels between the original article and the present work. We have not attempted to relabel published energy level data. The agreement seen on all figures confirms the high accuracy of the previous determinations of the energy levels and that of the present MARVEL analysis.

Finally, the present MARVEL results are compared to those of Toth [229] in Fig. 8. As observed repeatedly, the agreement is impressive below about 5000 cm^{-1}. Above this, the agreement becomes somewhat poorer due probably at least partially to the inclusion of emission results in the present MARVEL analysis. Comparisons of the MARVEL energy levels with other (partial) compilations of energy levels are given as a dynamic figure in the supplementary data.
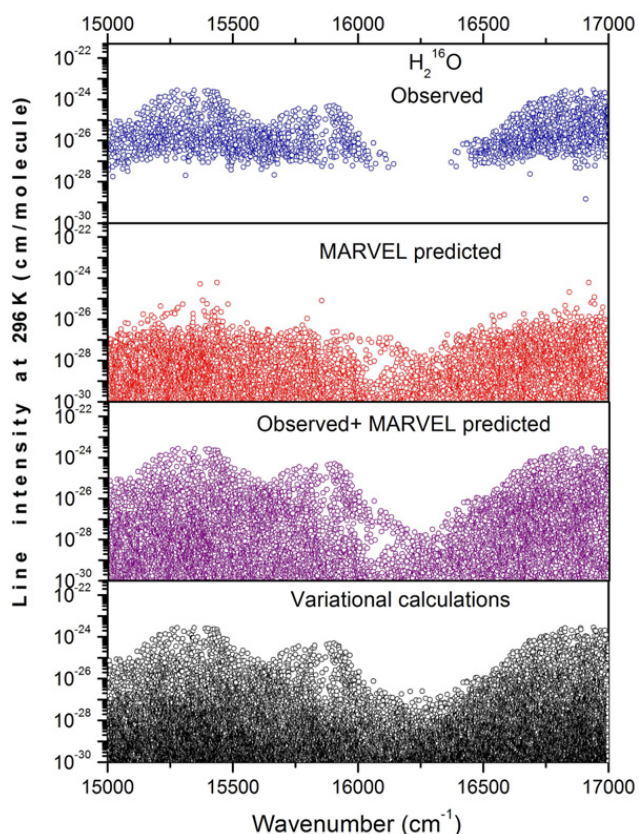
Fig. 4. An expanded view of Fig. 3 comparing intensities at 296 K for absorption transitions of $H_2^{16}O$: 15 000–17 000 cm^{-1}.
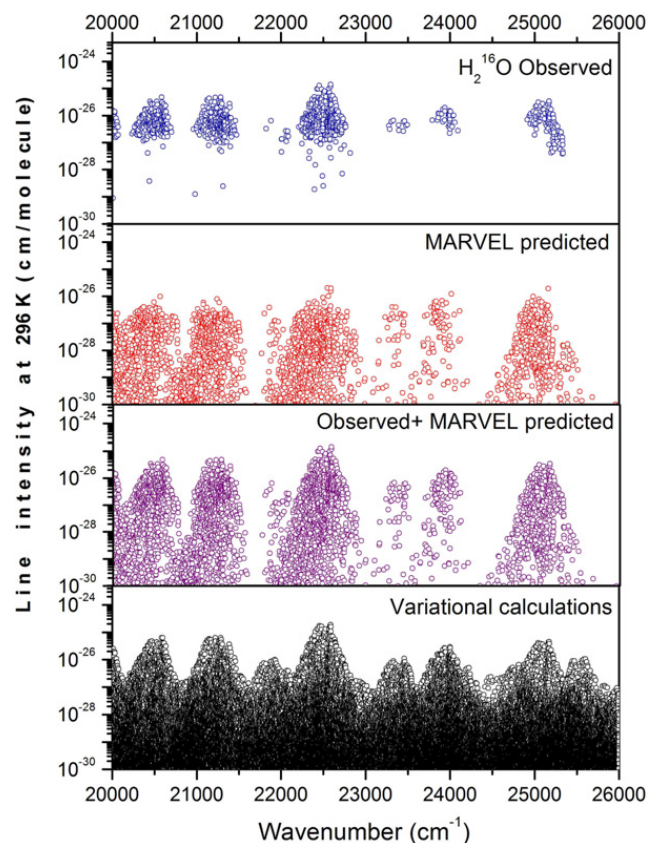
Fig. 5. An expanded view of Fig. 3 comparing intensities at 296 K for absorption transitions of $H_2^{16}O$: 20 000–26 000 cm^{-1}.

4. A comparison with HITRAN and HITEMP

The relevant features of the HITRAN database [225,235] are summarized in the original publication and in Part I; thus, they are not repeated here in detail, just a few remarks are made.

For a discussion of comparisons of the results of the present IUPAC-sponsored work (transition wavenumbers and energy levels) with data archived in HITRAN, it is worth recalling the structure of and quantities in the current edition of the HITRAN database [225]. Table 2 of Ref. [225] presents the parameters (fields) that are contained in each transition (record) of the HITRAN linelist. The structure is in a text-file format of fixed-length records. The parameters contained in each transition are those that have been deemed necessary for input for calculating high-resolution absorption or radiance spectra through room-temperature gaseous media. There are 36 550 assigned transitions of $H_2^{16}O$ (and an additional 882 unassigned transitions for this isotopologue) in the current edition of the HITRAN database [225] from 0 to 25 300 cm^{-1}. The values for the line positions of different transitions originate from a wide variety of sources which are documented by means of a special reference index. Unlike the MARVEL database, HITRAN contains both experimental and calculated values and also provides only one chosen value for each transition. Table 8 provides statistics on the number of transitions in the MARVEL and HITRAN databases and how many of them

are unique for the former set. One can see that there are 4599 assigned transitions in HITRAN that are not present in the MARVEL database or, in other words, have never been measured directly (or at least not published in the refereed works). This is not surprising because HITRAN contains data that are often calculated using (1) spectroscopic constants that are derived from fitting experimental spectra (for instance data in the 0–500 cm^{-1} region originate from Ref. [124]), and (2) energy differences between empirically determined levels. For instance, there are 4976 transitions in HITRAN that originate from the SISAM database [229] which are calculated by the second method. Unlike the case of some other water isotopologues, there are no line positions in HITRAN for the parent isotopologue that are computed variationally using *ab initio* PESs.

One of the most valuable results of this IUPAC effort is that by using validated empirical energy levels, in the present case MARVEL ones, one can generate an extensive database of line positions of all allowed transitions between such levels. Of course, the number of such transitions is extremely large, and although they are allowed, some of them will be very weak even under extreme thermodynamic conditions and are unlikely to be observed experimentally even in emission. Table 9 compares the database created from MARVEL energy-level differences with HITRAN. In general there is a very good agreement, although some differences exist and they need

Table 7

Reproduction of experimental transition data in the THz region, given in MHz, by MARVEL energy levels of A^+ quality for $H_2^{16}O$. The uncertainties, given in parentheses, are in kHz.

Transition	MARVEL	11DrYuPeGu [162]	06MaToNaMo [146]	04CoPiVeLa [135]	95MaOdIwTs [104]
$(0\ 1\ 0)\ 7_{25}-7_{16}$	2 484 150.788(1587)	2 484 150.996(200)	2 484 151.226(900)	2 484 153.205(26 981)	2 484 150.917(90)
$(0\ 1\ 0)\ 4_{31}-4_{22}$	2 488 754.576(321)	2 488 754.611(200)	2 488 755.140(900)	2 488 737.632(26 981)	2 488 754.284(254)
$(0\ 1\ 0)\ 4_{32}-5_{05}$	2 519 730.177(2508)	2 519 730.240(300)	2 519 730.570(900)		2 519 730.252(1050)
$(0\ 0\ 1)\ 6_{42}-6_{61}$	2 527 955.302(426)	2 527 953.387(200)			
$(0\ 0\ 0)\ 9_{37}-8_{44}$	2 531 916.820(573)	2 531 917.711(100)	2 531 918.154(900)	2 531 919.444(26 981)	2 531 917.811(46)
$(0\ 1\ 0)\ 6_{24}-5_{33}$	2 541 728.504(910)	2 541 728.011(300)	2 541 728.115(900)	2 541 760.432(26 981)	2 541 727.798(360)
$(0\ 0\ 0)\ 9_{46}-8_{53}$	2 547 373.945(670)	2 547 436.364(100)	2 547 457.389(900)		
$(0\ 0\ 0)\ 11_{47}-11_{38}$	2 571 763.702(472)	2 571 762.770(150)	2 571 762.976(900)	2 571 733.087(26 981)	2 571 762.630(26)
$(0\ 0\ 0)\ 10_{38}-9_{45}$	2 575 003.775(419)	2 575 004.568(150)	2 575 004.992(900)	2 574 995.429(26 981)	2 575 004.634(88)
$(0\ 0\ 0)\ 8_{36}-9_{09}$	2 576 642.908(2152)	2 576 644.123(150)			
$(0\ 1\ 0)\ 9_{36}-9_{27}$	2 586 380.933(2146)	2 586 380.418(300)	2 586 380.529(900)	2 586 390.841(26 981)	2 586 380.192(202)
$(0\ 1\ 0)\ 4_{23}-4_{14}$	2 590 793.198(238)	2 590 792.123(100)	2 590 792.515(900)	2 590 797.491(26 981)	2 590 792.169(96)
$(0\ 2\ 0)\ 5_{14}-5_{05}$	2 592 247.024(1944)	2 592 222.980(500)	2 592 250.885(901)		
$(0\ 0\ 0)\ 13_{310}-14_{213}$	2 602 480.453(3938)	2 602 480.635(250)			
$(0\ 0\ 0)\ 10_{56}-9_{63}$	2 618 252.725(373)	2 618 261.346(100)			
$(0\ 0\ 0)\ 9_{27}-10_{110}$	2 619 336.116(3000)	2 619 334.263(150)			
$(0\ 0\ 0)\ 5_{33}-5_{24}$	2 630 959.170(290)	2 630 959.639(100)	2 630 959.883(900)	2 630 947.502(26 981)	2 630 959.520(54)
$(0\ 0\ 0)\ 4_{14}-3_{03}$	2 640 464.849(450)	2 640 473.813(3)	2 640 474.218(900)		2 640 473.836(32)
$(0\ 1\ 0)\ 3_{30}-3_{21}$	2 646 587.344(1733)	2 646 587.356(200)	2 646 587.617(900)	2 646 570.289(26 981)	2 646 587.259(690)
$(0\ 0\ 0)\ 4_{41}-5_{14}$	2 657 665.849(501)	2 657 665.795(100)			
$(0\ 0\ 0)\ 7_{43}-7_{34}$	2 664 569.423(274)	2 664 570.803(100)	2 664 571.089(900)	2 664 573.428(26 981)	2 664 570.704(32)
$(0\ 0\ 0)\ 5_{24}-5_{15}$	2 685 639.319(260)	2 685 638.984(100)	2 685 639.337(900)	2 685 659.933(26 981)	2 685 638.969(36)
$(0\ 1\ 0)\ 4_{14}-3_{03}$	2 689 143.381(474)	2 689 142.009(100)	2 689 142.502(900)	2 689 147.119(26 981)	2 689 142.154(282)
$(0\ 0\ 0)\ 11_{65}-10_{74}$	2 689 170.506(833)	2 689 169.829(250)			
$(0\ 0\ 0)\ 12_{76}-11_{83}$	2 714 158.873(3210)	2 714 160.346(250)	2 714 157.309(26 981)		
$(0\ 0\ 0)\ 12_{75}-11_{84}$	2 723 387.539(7959)	2 723 411.903(300)			

to be studied carefully. One should note that there is a problem of correspondence between quantum assignments of energy levels given in the HITRAN and MARVEL lists. This is due to the fact that only the rotational quantum number J and symmetry (cf. Table 1) can be unambiguously identified using theoretical approaches. The different experimental works that contributed to HITRAN have used techniques and conventions to aid in the assignments of the observed transitions, which can result in labeling ambiguities. Therefore, although Table 9 shows that there are 1068 transitions that differ by more than 0.1 cm^{-1}, a few hundred of such transitions are in a category of different assignments and do not necessarily indicate problems in the HITRAN line positions. It is planned to revisit the labeling of energy levels in a future release of HITRAN; this issue is of particular importance since the algorithm used by HITRAN to generate pressure-broadening parameters is based on the quantum numbers [231].

It is worth noting that the database of transitions generated from MARVEL energy levels can prove extremely useful in updating the HITEMP database [29] and the *ab initio* line positions adopted from the BT2 line list [194]. In fact, when the HITEMP database was put together, a similar effort had been carried out but the database of transitions generated from experimental energy levels was significantly less complete (by more than a million transitions) and had not undergone a rigorous validation procedure. That being said, there are 114 209 395 transitions of $H_2^{16}O$ in the current edition of the HITEMP database [29], and the majority of line positions will still remain to be of *ab initio* origin.

5. Conclusions

Among many other applications of such data, an extreme quantity of high-quality molecular data are needed to understand properties of spectroscopic measurements related to different stars and the atmospheres of planets and exoplanets [232]. At the same time, non-thermodynamic equilibrium spectroscopic sources, such as water masers [9], are sensitive to thermally strongly suppressed transitions and probe a few, selected, high-lying energy levels. Such applications require knowledge of precise positions and often times intensities and line shapes to extract information such as chemical composition and pressure–temperature profiles. Thus, studies of the complete spectra of the water isotopologues are of prime importance. Furthermore, the high-resolution rovibrational spectra of the isotopologues of the water molecule form a fertile test ground for different experimental and theoretical approaches, like the present IUPAC effort, yielding the required information.

While the ambitious task of the IUPAC TG partially responsible for this work is to obtain a complete linelist for all isotopologues of water, a first step is to determine energy levels and line positions. This paper provides a dependable and carefully validated set of energy levels and transition wavenumbers, all with dependable and self-consistent uncertainties and labels, for the parent isotopologue, $H_2^{16}O$. The uncertainties produced by this work, due to the algorithm used, are usually larger for the energy levels than the underlying errors. This is something that should be investigated in future work.
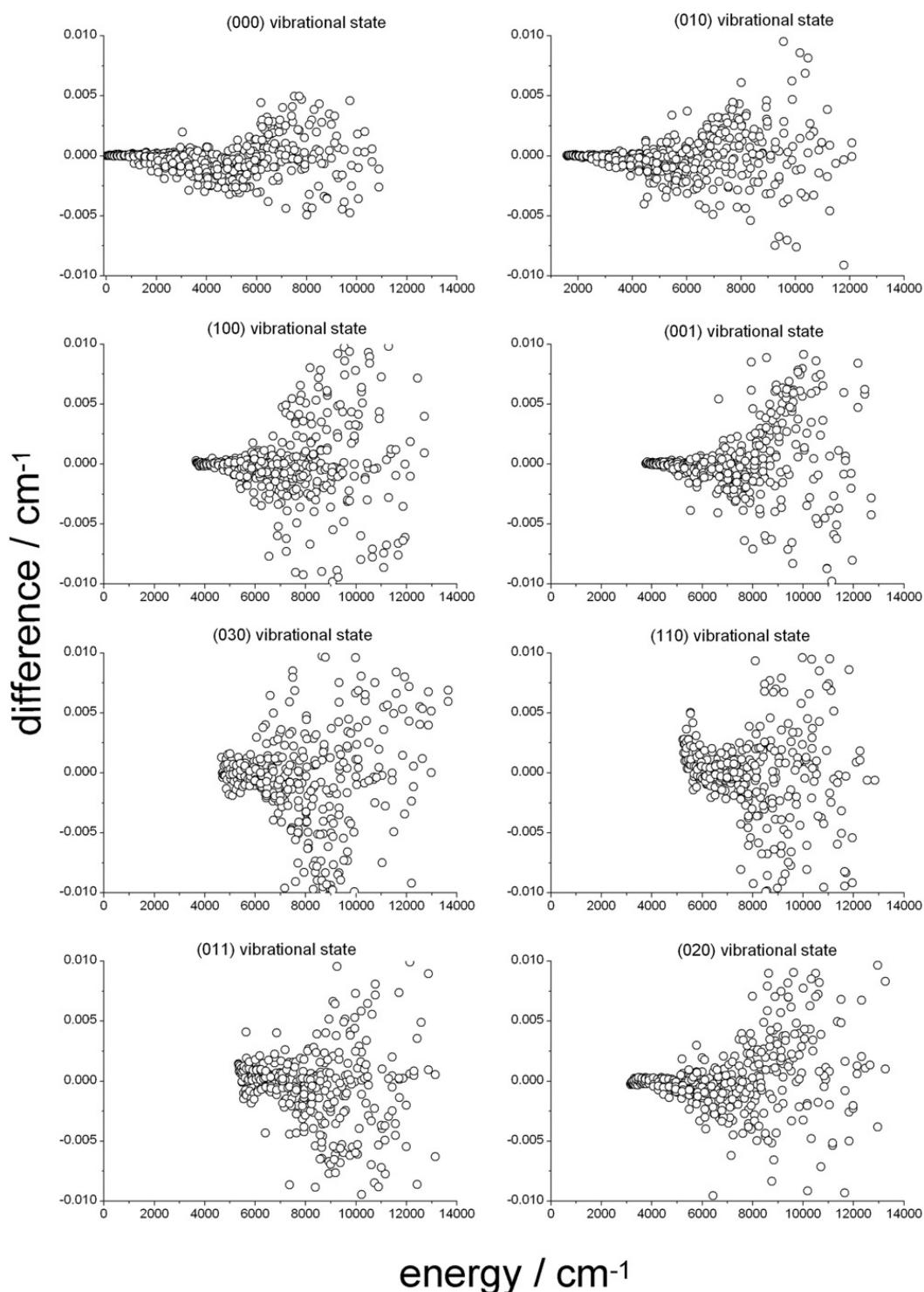
Fig. 6. Differences between MARVEL and empirical, effective-Hamiltonian-based energy levels from 04CoPiVeLa [135] for the eight lowest-energy vibrational states of $H_2^{16}O$.

As proven in this work, the MARVEL approach [23,25–27], combined with results from variational nuclear motion computations, provides an ideal platform to achieve the goal of producing accurate energy levels not only for $H_2^{16}O$ but for other molecules, as well.

An important aspect of the work presented here relies on recent advances in the *ab initio* calculation of dipole

moment surfaces and hence accurate transition intensities [49,233]. Transition intensities computed using a high quality *ab initio* dipole moment surface have been proven to be reliable and competitive with the best laboratory measurements in nearly all cases, although possible issues still remain [160]. This situation is certainly not true for the *ab initio* calculation of transition frequencies
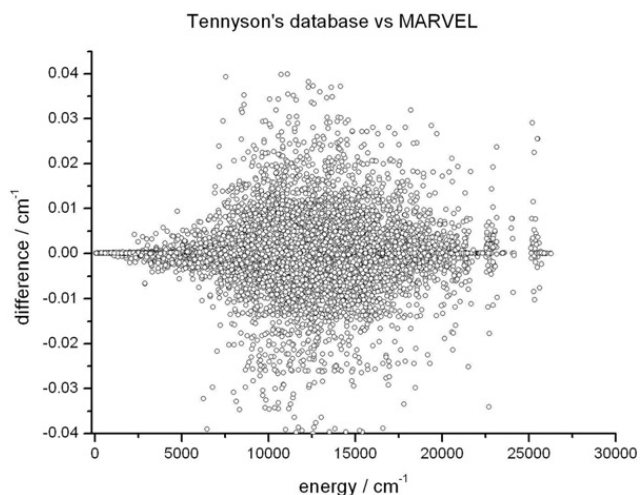
Fig. 7. Differences between the present MARVEL and a previous large set of "measured" energy levels compiled in Ref. [28] for $H_2^{16}O$.
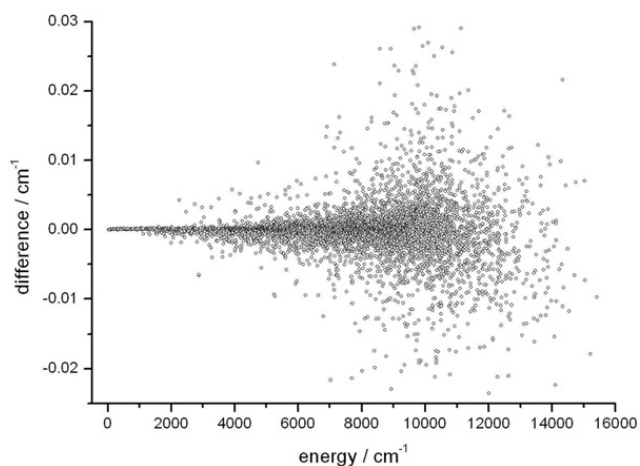
Fig. 8. Differences between the present MARVEL and a previous large set of "mixed" energy levels compiled in Ref. [229] (SISAM) for $H_2^{16}O$.

Table 8
Comparison of $H_2^{16}O$ transition found in HITRAN [225] and used in the present compilation for 298 K.

Total number of transitions in present database	184 667
Number of unique transitions in present database	100 459
Number of validated transitions	182 156
Assigned unique transitions in HITRAN database	36 550
Concordant transitions[a]	31 951
Transitions absent in present database[b]	4599

[a] Unique transitions which are present both in HITRAN and in the present validated IUPAC database.
[b] These transitions within HITRAN most likely correspond to computed and not to measured results.

[187]. This means that the combination of MARVEL line positions and *ab initio* line intensities can be used to give highly accurate spectroscopic parameters. A first study using this approach has recently been completed for $H_2^{18}O$ and $H_2^{17}O$ [234]; the present data provides the starting point for a similar study on the main isotopologue, $H_2^{16}O$, for which there remains a number of issues obtaining reliable spectroscopic data for purposes such as atmospheric monitoring [235].

The distributed information system W@DIS [236,237], one of the intended end products of the effort of this IUPAC TG, can be accessed via http://wadis.saga.iao.ru/ and contains the data forming the basis of this paper.

Acknowledgments

Appendix A. Supplementary data

Supplementary data associated with this article can be found in the online version at http://dx.doi.org/10.1016/j.jqsrt.2012.10.002.

Table 9
Comparison of $H_2^{16}O$ MARVEL-based one-photon absorption transition data and those found in HITRAN [230].

Total number of transitions generated from MARVEL database of energy levels	5 046 272
Concordant transitions with HITRAN[a]	36 369
Transitions differing by > 0.001 cm^{-1}	10 772
Transitions differing by > 0.01 cm^{-1}	2021
Transitions differing by > 0.1 cm^{-1}	1068
HITRAN transitions absent in database of transitions generated from MARVEL database of energy levels	181

[a] Unique transitions which are present both in HITRAN [225] and in the present validated IUPAC database.

References

[1] Wayne RP. Chemistry of atmospheres. 3rd ed.. New York: Oxford University Press; 2000.

[2] Bernath PF. The spectroscopy of water vapour: experiment, theory and applications. Phys Chem Chem Phys 2002;4:1501–9.

[3] Maksyutenko P, Grechko M, Rizzo TR, Boyarkin OV. State-resolved spectroscopy of high vibrational levels of water up to the dissociative continuum. Philos Trans R Soc A 2012:2710–27.

[4] Lodi L, Tennyson J. Theoretical methods for small-molecule ro-vibrational spectroscopy. J Phys B: At Mol Opt Phys 2010;43: 13301.

[5] Polyansky OL, Zobov NF, Mizus II, Lodi L, Yurchenko SN, Tennyson J, et al. Global spectroscopy of the water monomer. Philos Trans R Soc London A 2012:2728–48.

[6] Tennyson J, Shine KP. Water in the gas phase: preface. Philos Trans R Soc London A 2012;370:2491–4.

[7] Varshalovich DA, Ivanchik AV, Babkovskaya NS. The $\lambda_0 = 1.35$ cm H_2O maser line: the hyperfine structure and profile asymmetry. Astron Lett 2006;32:29–38.

[8] Vlemmings WHT, van Langevelde HJ, Diamond PJ. The magnetic field around late-type stars revealed by the circumstellar H_2O masers. Astron Astrophys 2005;434:1029–38.

[9] Caswell JL, Breen SL, Ellingsen SP. A water maser survey towards the galactic centre. Mon Not R Astron Soc 2011;410:1283–94.

[10] Bockelée-Morvan D, Biver N, Colom P, Crovisier J, Henry F, Lecacheux A, et al. The outgassing and composition of Comet 19P/Borrelly from radio observations. Icarus 2004;167:113–28.

[11] Biver N, Lecacheux A, Encrenaz T, Lellouch E, Baron P, Crovisier J, et al. Wide-band observations of the 557 GHz water line in Mars and Odin. Astron Astrophys 2005;435:765–72.

[12] Tinetti G, Vidal-Madjar A, Liang M-C, Beaulieu J-P, Yung Y, Carey S, et al. Water vapour in the atmosphere of a transiting extrasolar planet. Nature 2007;448:169–71.

[13] Allard F, Hauschildt PH, Miller S, Tennyson J. The influence of H_2O line blanketing on the spectra of cool dwarf stars. Astrophys J 1994;426:L39–41.

[14] Decin L, Agundez M, Barlow MJ, Daniel F, Cernicharo J, Lombaert R, et al. Warm water vapour in the sooty outflow from a luminous carbon star. Nature 2010;467:64–7.

[15] Cernicharo J, Pardo J, Gonzalez-Alfonso E, Serabyn E, Phillips T, Benford D, et al. Physical conditions in shocked regions of Orion from ground-based observations of H_2O. Astrophys J 1999;520: L131–4.

[16] Combes F, Wiklind T. Detection of water at $z = 0.685$ toward B0218+357. Astrophys J 1997;486(2, Part 2):L79–82.

[17] Lisak D, Havey DK, Hodges JT. Spectroscopic line parameters of water vapor for rotation–vibration transitions near 7180 cm^{-1}. Phys Rev A 2009;79:052507.

[18] Vidler M, Tennyson J. Accurate partition function and thermodynamic data for water. J Chem Phys 2000;113:9766–71.

[19] Hall RJ, Shirley JA. Coherent anti-Stokes Raman spectroscopy of water vapor for combustion diagnostics. Appl Spectrosc 1983;37:196–202.

[20] Tennyson J, Bernath PF, Brown LR, Campargue A, Carleer MR, Császár AG, et al. Critical evaluation of the rotational–vibrational spectra of water vapor. Part I. Energy levels and transition wavenumbers for $H_2^{17}O$ and $H_2^{18}O$. J Quant Spectrosc Radiat Transfer 2009;110:573–96.

[21] Palenikova J, Kraus M, Neogrady P, Kelloe V, Urban M. Theoretical study of molecular properties of low-lying electronic excited states of H_2O and H_2S. Mol Phys 2008;106:2333–44.

[22] Tennyson J, Bernath PF, Brown LR, Campargue A, Carleer MR, Császár AG, et al. Critical evaluation of the rotational–vibrational spectra of water vapor. Part II. Energy levels and transition wavenumbers for HD^{16}O, HD^{17}O, and HD^{18}O. J Quant Spectrosc Radiat Transfer 2010;110:2160–84.

[23] Császár AG, Czakó G, Furtenbacher T, Mátyus E. An active database approach to complete spectra of small molecules. Ann Rep Comput Chem 2007;3:155–76.

[24] Császár AG, Furtenbacher T. Spectroscopic networks. J Mol Spectrosc 2011;266:99–103.

[25] Furtenbacher T, Császár A, Tennyson J. MARVEL: measured active rotational–vibrational energy levels. J Mol Spectrosc 2007;245: 115–25.

[26] Furtenbacher T, Császár AG. On employing $H_2^{16}O$, $H_2^{17}O$, $H_2^{18}O$, and $D_2^{16}O$ lines as frequency standards in the 15–170 cm^{-1} window. J Quant Spectrosc Radiat Transfer 2008;109:1234–51.

[27] Furtenbacher T, Császár AG. MARVEL: measured active rotational–vibrational energy levels. II. Algorithmic improvements. J Quant Spectrosc Radiat Transfer 2012;113:929–35.

[28] Tennyson J, Zobov NF, Williamson R, Polyansky OL, Bernath PF. Experimental energy levels of the water molecule. J Phys Chem Ref Data 2001;30:735–831.

[29] Rothman LS, Gordon IE, Barber RJ, Dothe H, Gamache RR, Goldman A, et al. HITEMP, the high-temperature molecular spectroscopic database. J Quant Spectrosc Radiat Transfer 2010;111:2139–50.

[30] Callegari A, Theule P, Tolchenov RN, Zobov NF, Polyansky OL, Tennyson J, et al. Dipole moments of highly vibrationally excited water. Science 2002;297:993–5.

[31] Maksyutenko P, Rizzo TR, Boyarkin OV. A direct measurement of the dissociation energy of water. J Chem Phys 2006;125:181101.

[32] Maksyutenko P, Zobov NF, Shirin SV, Polyansky OL, Muenter JS, Rizzo TR, et al. Approaching the full set of energy levels of water. J Chem Phys 2007;126:241101.

[33] Grechko M, Maksyutenko P, Zobov NF, Shirin SV, Polyansky OL, Rizzo TR, et al. Collisionally assisted spectroscopy of water from 27 000 to 34 000 cm^{-1}. J Phys Chem A 2008;112:10539–45.

[34] Grechko M, Boyarkin OV, Rizzo TR, Maksyutenko P, Zobov NF, Shirin S, et al. State-selective spectroscopy of water up to its first dissociation limit. J Chem Phys 2009;131:221105.

[35] Grechko M, Maksyutenko P, Rizzo TR, Boyarkin OV. Communication: Feshbach resonances in the water molecule revealed by state-selective spectroscopy. J Chem Phys 2010;133:081103.

[36] Császár AG, Mátyus E, Szidarovszky T, Lodi L, Zobov NF, Shirin SV, et al. First-principles prediction and partial characterization of the vibrational states of water up to dissociation. J Quant Spectrosc Radiat Transfer 2010;111:1043–64.

[37] Zobov NF, Shirin SV, Lodi L, Shirin BC, Tennyson J, Császár AG, et al. First-principles rotation–vibration spectrum of water above dissociation. Chem Phys Lett 2011;507:48–51.

[38] Furtenbacher T, Császár AG. The role of intensities in determining characteristics of spectroscopic networks. J Mol Struct 2012;1009: 123–9.

[39] Jensen P. The potential energy surface for the electronic ground state of the water molecule determined from experimental data using a variational approach. J Mol Spectrosc 1989;133: 438–60.

[40] Polyansky OL, Jensen P, Tennyson J. A spectroscopically determined potential energy surface for the ground state of $H_2^{16}O$: a new level of accuracy. J Chem Phys 1994;101:7651–7.

[41] Polyansky OL, Jensen P, Tennyson J. The potential energy surfaces of $H_2^{16}O$. J Chem Phys 1996;105:6490–7.

[42] Partridge H, Schwenke DW. The determination of an accurate isotope dependent potential energy surface for water from extensive ab initio calculations and experimental data. J Chem Phys 1997;106:4618–39.

[43] Shirin SV, Polyansky OL, Zobov NF, Barletta P, Tennyson J. Spectroscopically determined potential energy surface of $H_2^{16}O$ up to 25 000 cm^{-1}. J Chem Phys 2003;118:2124–9.

[44] Shirin SV, Polyansky OL, Zobov NF, Ovsyannikov RI, Császár AG, Tennyson J. Spectroscopically determined potential energy surfaces of the $H_2^{16}O$, $H_2^{17}O$ and $H_2^{18}O$ isotopologues of water. J Mol Spectrosc 2006;236:216–23.

[45] Barletta P, Shirin SV, Zobov NF, Polyansky OL, Tennyson J, Valeev EF, et al. The CVRQD ab initio ground state potential surfaces for the water molecule. J Chem Phys 2006;125:204307.

[46] Bubukina II, Zobov NF, Polyansky OL, Shirin SV, Yurchenko SN. Optimized semiempirical potential energy surface for $H_2^{16}O$ up to 26000 cm^{-1}. Opt Spectrosc 2011;110:160–6.

[47] Schwenke DW, Partridge H. Convergence testing of the analytic representation of an ab initio dipole moment function for water: improved fitting yields improved intensities. J Chem Phys 2000;113: 6592–7.

[48] Lodi L, Tolchenov RN, Tennyson J, Lynas-Gray AE, Shirin SV, Zobov NF, et al. A high accuracy dipole surface for water. J Chem Phys 2008;128:044304.

[49] Lodi L, Tennyson J, Polyansky OL. A global, high accuracy *ab initio* dipole moment surface for the electronic ground state of the water molecule. J Chem Phys 2011;135:034113.

[50] Brown JM, Hougen JT, Huber KP, Johns JWC, Kopp I, Lefebvre-Brion H, et al. Labeling of parity doublet levels in linear molecules. J Mol Spectrosc 1975;55:500–3.

[51] Watson JKG. Robust weighting in least-squares fits. J Mol Spectrosc 2003;219:326–8.

[52] Golden S, Wentink T, Hillger RE, Strandberg MWP. Stark spectrum of H_2O. Phys Rev 1948;73:92–3.

[53] King WC, Gordy W. One-to-two millimeter wave spectroscopy. IV. Experimental methods and results for OCS, CH$_3$F, and H$_2$O. Phys Rev 1954;93:407–12.

[54] Dalby FW, Nielsen HH. Infrared spectrum of water vapor. Part I—the 6.26 μm region. J Chem Phys 1956;25:934–40.

[55] Hall RT, Dowling JM. Pure rotational spectrum of water vapor. J Chem Phys 1967;47:2454–61.

[56] Kukolich SG. Measurement of the molecular g values in H$_2$O and D$_2$O and hyperfine structure in H$_2$O. J Chem Phys 1969;50: 3751–5.

[57] Huiszoon C. A high resolution spectrometer for the shorter millimeter wavelength region. Rev Sci Instrum 1971;42:477–81.

[58] Steenbeckeliers G, Bellet J. Spectre micro-onde de molecules H$_2^{16}$O, H$_2^{17}$O et H$_2^{18}$O. CR Acad Sci Paris 1971;273:471–4.

[59] De Lucia FC, Helminger P, Cook RL, Gordy W. Submillimeter microwave spectrum of H$_2^{16}$O. Phys Rev A 1972;5:487–90.

[60] Flaud J-M, Camy-Peyret C, Valentin A. Spectre infrarouge a haute résolution des bandes $v_1 + v_2$ et $v_2 + v_3$ de H$_2^{16}$O. J Phys 1972;33: 741–7.

[61] Winton RS. Unpublished, PhD thesis. Duke University; 1972.

[62] Camy-Peyret C, Flaud J-M, Guelachvili G, Amiot C. High resolution Fourier transform spectrum of water between 2930 and 4255 cm^{-1}. Mol Phys 1973;26:825–55.

[63] Flaud JM, Camy-Peyret C. The $2v_2$, v_1 and v_3 bands of H$_2^{16}$O. Rotational study of the (000) and (020) states. Mol Phys 1973;26: 811–23.

[64] Pugh LA, Rao KN. Spectrum of water vapor in the 1.9 and 2.7 μm regions. J Mol Spectrosc 1973;47:403–8.

[65] Flaud J-M, Camy-Peyret C. Vibration-rotation intensities in H$_2$O-type molecules application to $2v_2$-band, v_1-band and v_3-band to H$_2^{16}$O. J Mol Spectrosc 1975;55:278–310.

[66] Flaud J-M, Camy-Peyret C, Narahari Rao K, Chen D-W, Hoh Y-S. Spectrum of water vapor between 8050 and 9370 cm^{-1}. J Mol Spectrosc 1979;75:339–62.

[67] Toth RA, Margolis JS. Line positions of H$_2$O in the 1.33 to 1.45 micron region. J Mol Spectrosc 1975;55:229–51.

[68] Flaud J-M, Camy-Peyret C, Maillard J-P, Guelachvili G. H$_2^{16}$O hot bands in the 6 μm region. Mol Phys 1977;34:413–26.

[69] Flaud J-M, Camy-Peyret C, Maillard J-P, Guelachvili G. The H$_2$O spectrum between 4200 and 5000 cm^{-1}. J Mol Spectrosc 1977;65: 219–28.

[70] Kauppinen J, Kakkainen T, Kyro E. High-resolution spectrum of water vapour between 30 and 720 cm^{-1}. J Mol Spectrosc 1978;71: 15–45.

[71] Lovas FJ. Microwave spectral tables. II. Triatomic molecules. J Phys Chem Ref Data 1978;7:1445–750.

[72] Flaud J-M, Camy-Peyret C, Rao KN, Chen D-W, Hoh Y-S. Spectrum of water vapor between 8050 and 9370 cm^{-1}. J Mol Spectrosc 1979;75:339–62.

[73] Herman M, Johns JWC, McKellar ARW. High resolution laser Stark and infrared–radiofrequency double resonance spectroscopy of H$_2^{16}$O at 6 μm. Can J Phys 1979;57:397–401.

[74] Camy-Peyret C, Flaud JM, Maillard J-P. The $4v_2$ band of H$_2^{16}$O. J Phys Lett 1980;41:L23–6.

[75] Kuze H. Microwave spectrum of water in the v_2 excited vibrational state. Astrophys J 1980;239:1131–3.

[76] Antipov AB, Bykov AD, Kapitanov VA, Lopasov VP, Makushkin YS, Tolmachev VI, et al. Water-vapor absorption spectrum in the 0.59-μm region. J Mol Spectrosc 1981;89:449–59.

[77] Kyrö E. Centrifugal distortion analysis of pure rotational spectra of H$_2^{16}$O, H$_2^{17}$O and H$_2^{18}$O. J Mol Spectrosc 1981;88:167–74.

[78] Partridge RH. Far-infrared absorption spectra of H$_2^{16}$O, H$_2^{17}$O and H$_2^{18}$O. J Mol Spectrosc 1978;87:429–37.

[79] Kauppinen J, Jomena K, Horneman V-M. New wavenumber calibration tables for H$_2$O, CO$_2$ and OCS lines between 400 cm^{-1} and 900 cm^{-1}. Appl Opt 1982;21:3332–6.

[80] Burenin AV, Fevralskikh TM, Karyakin EN, Polyansky OL, Shapin SM. Effective Pade Hamiltonian operator and its application for treatment of H$_2^{16}$O rotational spectrum in the ground state. J Mol Spectrosc 1983;100:182–92.

[81] Guelachvili G. Experimental Doppler-limited spectra of the v_2-bands of H$_2^{16}$O, H$_2^{17}$O, H$_2^{18}$O, and HDO by Fourier-transform spectroscopy – secondary wave-number standards between 1066 and 2296 cm^{-1}. J Opt Soc Am 1983;2:137–50.

[82] Helminger P, Messer JK, De Lucia FC. Continuously tunable coherent spectroscopy for the 0.1–1.0 THz region. Appl Phys Lett 1983;42:309–10.

[83] Pine AS, Coulombe MJ, Camy-Peyret C, Flaud J-M. Atlas of the high-temperature water vapor spectrum in the 3000 to 4000 cm^{-1} region. J Phys Chem Ref Data 1983;12:413–65.

[84] Brown LR, Toth RA. Comparison of the frequencies of NH$_3$, CO$_2$, H$_2$O, N$_2$O, CO, and CH$_4$ as infrared calibration standards. J Opt Soc Am B 1985;2:842–56.

[85] Camy-Peyret C, Flaud J-M, Mandin J-Y, Chevillard J-P, Brault J, Ramsay DA, et al. The high-resolution spectrum of water vapor between 16500 and 25250 cm^{-1}. J Mol Spectrosc 1985;113:208–28.

[86] Johns JWC. High-resolution far-infrared (20–350-cm^{-1}) spectra of several isotopic species of H$_2$O. J Opt Soc Am B 1985;2: 1340–54.

[87] Mandin J-Y, Chevillard J-P, Camy-Peyret C, Flaud J-M. The high-resolution spectrum of water-vapor between 13 200 and 16 500 cm^{-1}. J Mol Spectrosc 1986;116:67–190.

[88] Mandin J-Y, Chevillard J-P, Camy-Peyret C, Flaud J-M. Line intensities in the $v_1 + 2v_2$, $2v_2 + v_3$, $2v_1$, $v_1 + v_3$, $2v_3$, and $v_1 + v_2 + v_3 - v_2$ bands of H$_2^{16}$O, between 6300 and 7900 cm^{-1}. J Mol Spectrosc 1986;118:96–102.

[89] Baskakov OI, Alekseev VA, Alekseev EA, Polevoi BI. New submillimeter rotational lines of water and its isotopes. Opt Spektrosk 1987;63:1016–8.

[90] Belov SP, Kozin IN, Polyansky OL, Tretyakov MY, Zobov NF. Rotational spectrum of the H$_2^{16}$O molecule in the (010) excited vibrational state. J Mol Spectrosc 1987;126:113–7.

[91] Mandin JY, Chevillard JP, Flaud J-M, Camy-Peyret C. H$_2^{16}$O: line positions and intensities between 8000 and 9500 cm^{-1}: the second hexad of interacting vibrational states: ((OSO), (130), (031), (210), (Ill), (012)). Can J Phys 1988;66:997–1011.

[92] Chevillard J-P, Mandin J-Y, Flaud J-M, Camy-Peyret C. H$_2^{16}$O: line positions and intensities between 9500 and 11500 cm^{-1}. The interacting vibrational states (041), (220), (121), (022), (300), (201), (102), and (003). Can J Phys 1989;67:1065–84.

[93] Amano T, Scappini F. Millimeter-wave spectrum of rotationally excited H$_2$O. Chem Phys Lett 1991;182:93–5.

[94] Pearson JC, Anderson T, Herbst E, De Lucia FC, Helminger P. Millimeter- and submillimeter-wave spectrum of highly excited states of water. Astrophys J 1991;379:L41–3.

[95] Toth RA. v_2 band of H$_2^{16}$O—line strengths and transition frequencies. J Opt Soc Am B 1991;8:2236–55.

[96] Dana V, Mandin JY, Camy-Peyret C, Flaud J-M, Rothman LS. Rotational and vibrational dependences of collisional linewidths in the $nv_2 - (n-1)v_2$ hot bands of H$_2$O from Fourier-transform flame spectra. Appl Opt 1992;31:1179–84.

[97] Dana V, Mandin JY, Camy-Peyret C, Flaud J-M, Chevillard JP, Hawkins RL, et al. Measurements of collisional linewidths in the v_2 band of H$_2$O from Fourier-transform flame spectra. Appl Opt 1992;31:1928–36.

[98] Mandin JY, Dana V, Camy-Peyret C, Flaud J-M. Collisional widths of pure rotational transitions of H$_2$O from Fourier-transform flame spectra. J Mol Spectrosc 1992;152:179–84.

[99] Toth RA. $2v_2 - v_2$ and $2v_2$ bands of H$_2^{16}$O, H$_2^{17}$O, and H$_2^{18}$O: line positions and strengths. J Opt Soc Am B 1993;10:1526–44.

[100] Toth RA. $v_1 - v_2$, $v_3 - v_2$, v_1 and v_3 bands of H$_2^{16}$O: line positions and strengths. J Opt Soc Am B 1993;10:2006–29.

[101] Coudert LH. Analysis of the rotational levels of water and determination of the potential energy function for the bending v_2 mode. J Mol Spectrosc 1994;165:406–25.

[102] Toth RA. Measurements of H$_2^{16}$O: line positions and strengths: 11610 to 12861 cm^{-1}. J Mol Spectrosc 1994;166:176–83.

[103] Toth RA. Extensive measurements of H$_2^{16}$O: frequencies and strengths: 5750 to 7965 cm^{-1}. Appl Opt 1994;33:4852–67.

[104] Matsushima F, Odashima H, Iwasaki T, Tsunekawa S, Takagi K. Frequency measure of pure rotational transitions of H$_2$O from 0.6 to 5 THz. J Mol Struct 1995;352:371–8.

[105] Paso R, Horneman V-M. High-resolution rotational absorption spectra of H$_2^{16}$O, HD ^{16}O, and D$_2^{16}$O between 110 and 500 cm^{-1}. J Opt Soc Am B 1995;12:1813–38.

[106] Brown LR, Margolis JS. Empirical line parameters of NH$_3$ from 4791 to 5294 cm^{-1}. J Quant Spectrosc Radiat Transfer 1996;56: 283–94.

[107] Polyansky OL, Busler JR, Guo BJ, Zhang KQ, Bernath PF. The emission spectrum of hot water in the region between 370 and 930 cm^{-1}. J Mol Spectrosc 1996;176:305–15.

[108] Coudert LH. Analysis of the line positions and line intensities in the v_2 band of the water molecule. J Mol Spectrosc 1997;181:246–73.

[109] Natale PD, Lorini L, Inguscio M, Nolt IG, Park JH, Lonardo GD, et al. Accurate frequency measurement for H$_2$O and ^{16}O$_3$ in the 119 cm^{-1} OH atmospheric window. Appl Opt 1997;36:8526–32.

[110] Mikhailenko SN, Tyuterev VG, Keppler KA, Winnewisser BP, Winnewisser M, Mellau G, et al. The $2\nu_2$ band of water: analysis of new FTS measurements and high-K_a transitions and energy levels. J Mol Spectrosc 1997;184:330–49.

[111] Flaud J-M, Camy-Peyret C, Bykov A, Naumenko O, Petrova T, Scherbakov A, et al. The water vapor linestrengths between 11 600 and 12 750 cm^{-1}. J Mol Spectrosc 1997;185:211–21.

[112] Flaud J-M, Camy-Peyret C, Bykov A, Naumenko O, Petrova T, Scherbakov A, et al. The high-resolution spectrum of water vapor between 11 600 and 12 750 cm^{-1}. J Mol Spectrosc 1997;183:300–9.

[113] Toth RA. Water vapor measurements between 590 and 2582 cm^{-1}: line positions and strengths. J Mol Spectrosc 1998;190:379–96.

[114] Toth RA. Analysis of line positions and strengths of $H_2^{16}O$ ground and hot bands connecting to interacting upper states: (020), (100), and (001). J Mol Spectrosc 1999;194:28–42.

[115] Polyansky OL, Zobov NF, Viti S, Tennyson J. Water vapour line assignments in the near infrared. J Mol Spectrosc 1998;189:291–300.

[116] Carleer M, Jenouvrier A, Vandaele A-C, Bernath PF, Mérienne MF, Colin R, et al. The near infrared, optical and near ultraviolet overtone spectrum of water. J Chem Phys 1999;111:2444–50.

[117] Belmiloud D, Schermaul R, Smith K, Zobov NF, Brault J, Learner RCM, et al. New studies of the visible and near infra-red absorption by water vapour and some problems with the database. Geophys Res Lett 2000;27:3703–6.

[118] Brown LR, Plymate C. Experimental line parameters of the oxygen A band at 760 nm. J Mol Spectrosc 2000;199:166–79.

[119] Chen P, Pearson JC, Pickett HM, Matsuura S, Blake GA. Submillimeter-wave measurements and analysis of the ground and $\nu_2 = 1$ states of water. Astrophys J Suppl Ser 2000;128:371–85.

[120] Zobov NF, Belmiloud D, Polyansky OL, Tennyson J, Shirin SV, Carleer M, et al. The near ultraviolet rotation–vibration spectrum of water. J Chem Phys 2000;113:1546–52.

[121] Schermaul R, Learner RCM, Newnham DA, Williams RG, Ballard J, Zobov NF, et al. The water vapour spectrum in the region 8600–15000 cm^{-1}: experimental and theoretical studies for a new spectral line database I: Laboratory measurements. J Mol Spectrosc 2001;208:32–42.

[122] Schermaul R, Learner RCM, Newnham DA, Ballard J, Zobov NF, Belmiloud D, et al. The water vapour spectrum in the region 8600–15000 cm^{-1}: experimental and theoretical studies for a new spectral line database II: Construction and validation. J Mol Spectrosc 2001;208:43–50.

[123] Bykov A, Naumenko O, Sinitsa L, Voronin B, Flaud J-M, Camy-Peyret C, et al. High-order resonances in the water molecule. J Mol Spectrosc 2001;205:1–8.

[124] Lanquetin R, Coudert LH, Camy-Peyret C. High-lying rotational levels of water: an analysis of the energy levels of the five first vibrational states. J Mol Spectrosc 2001;206:83–103.

[125] Naus H, Ubachs W, Levert PF, Polyansky OL, Zobov NF, Tennyson J. Cavity-ring-down spectroscopy on water vapor in the range 555–604 nm. J Mol Spectrosc 2001;205:117–21.

[126] Brown LR, Toth RA, Dulick M. Empirical line parameters of $H_2^{16}O$ near 0.94 μm: positions, intensities, and air-broadening coefficients. J Mol Spectrosc 2002;212:57–82.

[127] Mikhailenko SN, Tyuterev VG, Starikov VI, Albert KK, Winnewisser BP, Winnewisser M, et al. Water spectra in the region 4200–6250 cm^{-1}; extended analysis of $\nu_1+\nu_2$, $\nu_2+\nu_3$, and $3\nu_2$ bands and confirmation of highly excited states from flame spectra and from atmospheric long-path observations. J Mol Spectrosc 2002;213:91–121.

[128] Schermaul R, Learner RCM, Canas AAD, Brault JW, Polyansky OL, Belmiloud D, et al. Weak line water vapor spectrum in the regions 13 200–15 000 cm^{-1}. J Mol Spectrosc 2002;211:169–78.

[129] Coheur PF, Fally S, Carleer M, Clerbaux C, Colin R, Jenouvrier A, et al. New water vapor line parameters in the 26 000–13 000 cm^{-1} region. J Quant Spectrosc Radiat Transfer 2002;74:493–510.

[130] Tolchenov RN, Tennyson J, Brault JW, Canas AAD, Schermaul R. Weak line water vapor spectrum in the 11,787–13,554 cm^{-1} region. J Mol Spectrosc 2002;215:269–74.

[131] Mérienne MF, Jenouvrier A, Hermans C, Vandaele AC, Carleer M, Clerbaux C, et al. Water vapor line parameters in the 13000–9250 cm^{-1} region. J Quant Spectrosc Radiat Transfer 2003;82:92–117.

[132] Naumenko O, Campargue A. Rovibrational analysis of the absorption spectrum of H_2O around 1.02 μm by ICLAS-VECSEL. J Mol Spectrosc 2003;221:221–6.

[133] Tolchenov RN, Tanaka M, Tennyson J, Zobov NF, Shirin SV, Polyansky OL, et al. Water line intensities in the near-infrared and visible. J Quant Spectrosc Radiat Transfer 2003;82:151–64.

[134] Tolchenov RN, Tennyson J, Shirin SV, Zobov NF, Polyansky OL, Maurellis AN. Water line parameters for weak lines in the range 9000–12 700 cm^{-1}. J Mol Spectrosc 2003;221:99–105.

[135] Coudert LH, Pirali O, Vervloet M, Lanquetin R, Camy-Peyret C. The eight first vibrational states of the water molecule: measurements and analysis. J Mol Spectrosc 2004;228:471–98.

[136] Macko P, Romanini D, Mikhailenko SN, Naumenko OV, Kassi S, Jenouvrier A, et al. High sensitivity CW-cavity ring down spectroscopy of water in the region of the $1.5 > $ μm atmospheric window. J Mol Spectrosc 2004;227:90–108.

[137] Bykov A, Naumenko O, Shcherbakov AP, Sinitsa L, Voronin BA. Identification and simulation of the $H_2^{16}O$ absorption spectrum in 5750–7965 cm^{-1} region. Atmos. Oceanic Opt. 2004;17:940–7.

[138] Horneman V-M, Anttila R, Alanko S, Pietila J. Transferring calibration from CO_2 laser lines to far infrared water lines with the aid of the ν_2 band of OCS and the ν_2, $\nu_1-\nu_2$, and $\nu_1+\nu_2$ bands of $^{13}CS_2$: molecular constants of $^{13}CS_2$. J Mol Spectrosc 2005;234:238–54.

[139] Toth RA. Measurements and analysis (using empirical functions for widths) of air- and self-broadening parameters of H_2O. J Quant Spectrosc Radiat Transfer 2005;94:1–50.

[140] Toth RA. Measurements of positions, strengths and self-broadened widths of H_2O from 2900 to 8000 cm^{-1}: line strength analysis of the 2nd triad bands. J Quant Spectrosc Radiat Transfer 2005;94:51–107.

[141] Tolchenov RN, Tennyson J. Water line parameters for weak lines in the range 7400–9600 cm^{-1}. J Mol Spectrosc 2005;231:23–7.

[142] Tolchenov RN, Zobov NF, Shirin SV, Polyansky OL, Tennyson J, Naumenko O, et al. Water vapor line assignments in the 9250–26000 cm^{-1} frequency range. J Mol Spectrosc 2005;233:68–76.

[143] Kassi S, Macko P, Naumenko O, Campargue A. The absorption spectrum of water near 750 nm by CW-CRDS: contribution to the search of water dimer absorption. Phys Chem Chem Phys 2005;7:2460–7.

[144] Dupré P, Gherman T, Zobov NF, Tolchenov RN, Tennyson J. Continuous-wave cavity ringdown spectroscopy of the 8ν polyad of water in the 25195–25340 cm^{-1} range. J Chem Phys 2005;123:154307.

[145] Golubiatnikov GY, Markov VN, Guarnieri A, Knöchel R. Hyperfine structure of $H_2^{16}O$ and $H_2^{18}O$ measured by Lamb-dip technique in the 180–560 GHz frequency range. J Mol Spectrosc 2006;240:251–4.

[146] Matsushima F, Tomatsu N, Nagai T, Moriwaki Y, Takagi K. Frequency measurement of pure rotational transitions in the $\nu_2 = 1$ state of H_2O. J Mol Spectrosc 2006;235:190–5.

[147] Mazzotti F, Naumenko OV, Kassi S, Bykov AD, Campargue A. ICLAS of weak transitions of water between 11300 and 12850 cm^{-1}: Comparison with FTS databases. J Mol Spectrosc 2006;239:174–81.

[148] Petrova T, Poplavskii Y, Serdukov V, Sinitsa L. Intracavity laser spectroscopy of high-temperature water vapour in the range 9390–9450 cm^{-1}. Mol Phys 2006;104:2692–700.

[149] Cazzoli G, Puzzarini C, Buffa G, Tarrini O. Experimental and theoretical investigation on pressure-broadening and pressure-shifting of the 22.2 GHz line of water. J Quant Spectrosc Radiat Transfer 2007;105:438–49.

[150] Jenouvrier A, Daumont L, Régalia-Jarlot L, Tyuterev VG, Carleer M, Vandaele AC, et al. Fourier transform measurements of water vapor line parameters in the 4200–6600 cm^{-1} region. J Quant Spectrosc Radiat Transfer 2007;105:326–55.

[151] Lisak D, Hodges JT. High-resolution cavity ring-down spectroscopy measurements of blended H_2O transitions. Appl Phys B 2007;88:317–25.

[152] Mikhailenko SN, Le W, Kassi S, Campargue A. Weak water absorption lines around 1.455 and 1.66 μm by CW-CRDS. J Mol Spectrosc 2007;244:170–8.

[153] Cazzoli G, Puzzarini C, Buffa G, Tarrini O. Pressure-broadening in the THz region: the 1.113 THz line of water. J Quant Spectrosc Radiat Transfer 2008;109:1563–74.

[154] Cazzoli G, Puzzarini C, Buffa G, Tarrini O. Pressure-broadening of water lines in the THz frequency region: improvements and confirmations for spectroscopic databases. Part I. J Quant Spectrosc Radiat Transfer 2008;109:2820–31.

[155] Tolchenov RN, Tennyson J. Water Line Parameters from Refitted Spectra constrained by empirical upper state levels: study of the 9500–14500 cm^{-1} region. J Quant Spectrosc Radiat Transfer 2008;109:559–68.

[156] Lisak D, Hodges JT. Low-uncertainty H_2O line intensities for the 930-nm region. J Mol Spectrosc 2008;249:6–13.

[157] Campargue A, Mikhailenko S, Liu AW. ICLAS of water in the 770 nm transparency window (12746–13558 cm^{-1}). Comparison with current experimental and calculated databases. J Quant Spectrosc Radiat Transfer 2008;109:2832–45.

[158] Cazzoli G, Puzzarini C, Buffa G, Tarrini O. Pressure-broadening of water lines in the THz frequency region: Improvements and confirmations for spectroscopic databases. Part II. J Quant Spectrosc Radiat Transfer 2009;110:609–18.

[159] Cazzoli G, Puzzarini C, Harding ME, Gauss J. The hyperfine structure in the rotational spectrum of water: lamb-dip technique and quantum-chemical calculations. Chem Phys Lett 2009;473:21–5.

[160] Liu A, Naumenko O, Kassi S, Campargue A. High sensitivity CW-CRDS of ^{18}O enriched water near 1.6 μm. J Quant Spectrosc Radiat Transfer 2009;110:1781–800.

[161] Beguier S, Mikhailenko S, Campargue A. The absorption spectrum of water between 13 540 and 14 070 cm^{-1}: ICLAS detection of weak lines and a complete line list. J Mol Spectrosc 2011;265:106–9.

[162] Drouin BJ, Yu SS, Pearson JC, Gupta H. Terahertz spectroscopy for space applications: 2.5–2.7 THz spectra of HD, H_2O and NH_3. J Mol Struct 2011;1006:2–12.

[163] Mikhailenko S, Kassi S, Wang L, Campargue A. The absorption spectrum of water in the 1.25 μm transparency window (7408–7920 cm^{-1}). J Mol Spectrosc 2011;269:92–103.

[164] Yu S, Pearson JC, Drouin BJ, Martin-Drumel M-A, Pirali O, Vervloet M, et al. Measurement and analysis of new tetrahertz and far-infrared spectra of high temperature water. J Mol Spectrosc 2012;113:2155–66.

[165] Leshchishina O, Mikhailenko S, Mondelain D, Kassi S, Campargue A. CRDS of water vapor at 0.1 Torr between 6886 and 7406 cm^{-1}. J Quant Spectrosc Radiat Transfer, in press.

[166] Camy-Peyret C, Flaud J-M, Maillard JP, Guelachvili G. Spectrum of water vapor between 8050 and 9370 cm^{-1}. Mol Phys 1977;33:1641–50.

[167] Polyansky OL, Tennyson J, Bernath PF. The spectrum of hot water: rotational transitions and difference bands in the (020), (100) and (001). J Mol Spectrosc 1997;186:213–21.

[168] Polyansky OL, Zobov NF, Viti S, Tennyson J, Bernath PF, Wallace L. High temperature rotational transitions of water in sunspot and laboratory spectra. J Mol Spectrosc 1997;186:422–47.

[169] Polyansky OL, Zobov NF, Tennyson J, Lotoski JA, Bernath PF. Hot bands of water in the v_2 manifold up to $5v_2 - 4v_2$. J Mol Spectrosc 1997;184:35–50.

[170] Esplin MP, Wattson RB, Hoke LB, Rothman LS. High-temperature spectrum of H_2O in the 720–1400 cm^{-1} region. J Quant Spectrosc Radiat Transfer 1998;60:711–39.

[171] Zobov NF, Polyansky OL, Tennyson J, Lotoski JA, Colarusso P, Zhang K-Q, et al. Hot bands of water up to $6v_2 - 5v_2$ in the 933–2500 cm^{-1} region. J Mol Spectrosc 1999;193:118–36.

[172] Zobov NF, Polyansky OL, Tennyson J, Shirin SV, Nassar R, Hirao T, et al. Using laboratory spectroscopy to identify lines in the K and L-band spectrum of water in a sunspot. Astrophys J 2000;530:994–8.

[173] Tereszchuk K, Bernath PF, Zobov NF, Shirin SV, Polyansky OL, Libeskind NI, et al. Laboratory spectroscopy of hot water near 2-microns and sunspot spectroscopy in the H-band region. Astrophys J 2002;577:496–500.

[174] Coheur P-F, Bernath PF, Carleer M, Colin R, Polyansky OL, Zobov NF, et al. 3200 K laboratory emission spectrum of water. J Chem Phys 2005;122:074307.

[175] Zobov NF, Shirin SV, Polyansky OL, Tennyson J, Coheur P-F, Bernath PF, et al. Monodromy in the water molecules. Chem Phys Lett 2005;414:193–7.

[176] Zobov NF, Shirin SV, Polyansky OL, Barber RJ, Tennyson J, Coheur P-F, et al. Spectrum of hot water in the 2000–4750 cm^{-1} frequency range. J Mol Spectrosc 2006;237:115–22.

[177] Zobov NF, Shirin SV, Ovsannikov RI, Polyansky OL, Barber RJ, Tennyson J, et al. Spectrum of hot water in the 4750–13000 cm^{-1} frequency range. Mon Not R Astron Soc 2008;387:1093–8.

[178] Miani A, Tennyson J. Can ortho–para transitions for water be observed? J Chem Phys 2004;120:2732–9.

[179] Polyansky OL. One-dimensional approximation of the effective rotational Hamiltonian of the ground state of the water molecule. J Mol Spectrosc 1985;112:79–87.

[180] Burenin AV, Tyuterev VG. On the application of the effective rotational Pade Hamiltonian operator of the molecule. J Mol Spectrosc 1984;108:153–4.

[181] Burenin AV, Polyansky OL, Shapin SM. Application of Pade Hamiltonian operator for description of rotational spectrum of H_2X molecules. Opt i Spektrosc 1982;54:436–41.

[182] Tyuterev VG. The generating function approach to the formulation of the effective rotational Hamiltonian: a simple closed form model describing strong centrifugal distortion in water-type nonrigid molecules. J Mol Spectrosc 1992;151:97–129.

[183] Starikov VI, Tashkun SA, Tyuterev VG. Description of vibration–rotation energies of nonrigid triatomic molecules using the generating function method: bending states and second triad of water. J Mol Spectrosc 1992;151:130–47.

[184] Császár AG, Mills IM. Vibrational energy levels of water. Spectrochim Acta 1997;53A:1101–22.

[185] Coudert LH. Analysis of the rotational levels of water. J Mol Spectrosc 1991;154:427–42.

[186] Lanquetin R, Coudert LH, Camy-Peyret C. High-lying rotational levels of water: comparison of calculated and experimental energy levels for (000) and (010) up to $J = 25$ and 21. J Mol Spectrosc 1999;195:54–67.

[187] Polyansky OL, Császár AG, Shirin SV, Zobov NF, Barletta P, Tennyson J, et al. High accuracy ab initio rotation–vibration transitions of water. Science 2003;299:539–42.

[188] Császár AG, Allen WD, Schaefer III HF. In pursuit of the ab initio limit for conformational energy prototypes. J Chem Phys 1998;108:9751–64.

[189] Tarczay G, Császár AG, Klopper W, Szalay V, Allen WD, Schaefer III HF. The barrier to linearity of water. J Chem Phys 1999;110:11971–81.

[190] Valeev EF, Allen WD, Schaefer III HF, Császár AG. The second-order Moller–Plesset limit for the barrier to linearity of water. J Chem Phys 2001;114:2875–8.

[191] Polyansky OL, Zobov NF, Viti S, Tennyson J, Bernath PF, Wallace L. Water in the sun: line assignments based on variational calculations. Science 1997;277:346–9.

[192] Guelachvili G, Rao KN. Handbook of infrared standards. Orlando, FL, USA: Academic press; 1986.

[193] Flaud J-M, Camy-Peyret C, Bykov A, Naumenko O, Petrova T, Scherbakov A, et al. The high-resolution spectrum of water vapor between 11 600 and 12 750 cm^{-1}. J Mol Spectrosc 1997;183:300–9.

[194] Barber RJ, Tennyson J, Harris GJ, Tolchenov RN. A high accuracy synthetic linelist for hot water. Mon Not R Astron Soc 2006;368:1087–94.

[195] Child MS, Halonen L. Overtone frequencies and intensities in the local mode picture. Adv Chem Phys 1984;57:1–58.

[196] Lemus R. Vibrational excitations in $H_2^{16}O$ in the framework of a local model. J Mol Spectrosc 2004;225:73–92.

[197] Császár AG, Mátyus E, Lodi L, Zobov NF, Shirin SV, Polyansky OL, et al. Ab initio prediction and partial characterization of the vibrational states of water up to dissociation. J Quant Spectrosc Radiat Transfer 2010;111:1043–64.

[198] Mátyus E, Fábri C, Szidarovszky T, Czakó G, Allen WD, Császár AG. Assigning quantum labels to variationally computed rotational–vibrational eigenstates of polyatomic molecules. J Chem Phys 2010;133:034113.

[199] Szidarovszky T, Fábri C, Császár AG. The role of axis embedding on rigid rotor decomposition (RRD) analysis of variational rovibrational wave functions. J Chem Phys 2012;136:174112.

[200] Child MS, Weston T, Tennyson J. Quantum monodromy in the spectrum of H_2O and other systems: new insight into the level structures of quasi-linear molecules. Mol Phys 1999;96:371–9.

[201] Mussa HY, Tennyson J. Calculation of rotation–vibration states of water at dissociation. J Chem Phys 1998;109:10885–92.

[202] Gray SK, Goldfield EM. Highly excited bound and low-lying resonance states of H_2O. J Phys Chem 2001;105:2634–41.

[203] Li GH, Guo H. The vibrational level spectrum of H_2O (X_1A') from the Partridge–Schwenke potential up to the dissociation limit. J Mol Spectrosc 2001;126:90–7.

[204] Farantos SC, Tennyson J. Quantum and classical vibrational chaos in floppy molecules. J Chem Phys 1985;82:800–9.

[205] Polyansky OL, Zobov NF, Tennyson J, Lotoski JA, Bernath PF. Hot bands of water in the v_2 manifold up to $5v_2 - 4v_2$. J Mol Spectrosc 1997;184:35–50.

[206] Guelachvili G, Birk M, Bordé CJ, Brault JW, Brown LR, Carli B, et al. High resolution wavenumber standards for the infrared. J Mol Spectrosc 1996;177:164–79.

[207] Maki AG, Wells JS. New wave-number calibration tables from heterodyne frequency measurements. J Res Nat Inst Stand Technol 1992;97:409–70.

[208] Horneman VM. High accurate peak positions for calibration purposes with the lowest fundamental bands v_2 of N_2O and CO_2. J Mol Spectrosc 2007;241:45–50.

[209] Okubo S, Nakayama H, Iwakuni K, Inaba H, Sasada H. Absolute frequency list of the v_3-band transitions of methane at a relative uncertainty level of 10^{-11}. Opt Express 2011;19:23878–88.

[210] Falke S, Tiemann E, Lisdat C, Schnatz H, Grosche G. Transition frequencies of the D lines of ^{39}K, ^{40}K, and ^{41}K measured with a femtosecond laser frequency comb. Phys Rev A 2006;74:032503.

[211] Liao CC, Wu KY, Lien YH, Knoeckel H, Chui HC, Tiemann E, et al. Precise frequency measurements of $^{127}I_2$ lines in the wavelength region 750–780 nm. J Opt Soc Am B—Opt Phys 2010;27:1208–14.

[212] Robichaud DJ, Hodges JT, Maslowski P, Yeung LY, Okumura M, Miller CE, et al. High-accuracy transition frequencies for the O_2 a-band. J Mol Spectrosc 2008;251:27–37.

[213] Voronin BA, Naumenko OV, Tolchenov RN, Tennyson J, Fally S, Coheur P-F, et al. HDO absorption spectrum above 11 500 cm^{-1}: assignment and dynamics. J Mol Spectrosc 2007;244:87–101.

[214] Evenson KM, Jennings DA, Petersen FR. Tunable far-infrared spectroscopy. Appl Phys Lett 1984;44:576–8.

[215] Belov SP, Burenin AV, Gershtein LI, Korolikhin VV, Krupnov AF. High-sensitivity millimeter and submillimeter wide-range radio-spectroscopy of gases. Opt i Spektrosk 1973;35:295–302.

[216] Amano T, Amano T. Millimeter-wave spectrum of NCS radical in the ground $^2\Pi$ state. J Chem Phys 1991;95:2275–9.

[217] Drouin B, Maiwald F, Pearson J. Application of cascaded frequency multiplication to molecular spectroscopy. Rev Sci Instrum 2005;76:093113.

[218] Ahonen T, Alanko S, Anttila R, Koivusaari M, Paso R, Tolonen AM, et al. New calibration of the OCS v_2 band. In: Abstracts of the twelfth international conference on high resolution infrared and microwave spectroscopy. Dobris, Czechoslovakia; 1992.

[219] Wallace L, Bernath P, Livingston W, Hinkle K, Busler J, Guo BJ, et al. Water on the sun. Science 1995;268:1155–8.

[220] Wallace L, Livingston W, Hinkle K, Bernath P. Infrared spectral atlases of the sun from NOAO. Astrophys J Sup 1996;106:165–9.

[221] Polyansky OL, Zobov NF, Viti S, Tennyson J, Bernath PF, Wallace L. Water in the sun: line assignments based on variational calculations. Science 1997;277:346–9.

[222] Polyansky OL, Zobov NF, Viti S, Tennyson J, Bernath PF, Wallace L. K band spectrum of water in sunspots. Astrophys J 1997;489: L205–8.

[223] Guelachvili G. Absolute wavenumbers and molecular constants of the fundamental bands of $^{12}C\ ^{16}O$, $^{12}C^{17}O$, $^{12}C^{18}O$, $^{13}C\ ^{16}O$, $^{13}C^{18}O$ and of the 2-1 bands of $^{12}C\ ^{16}O$ and $^{13}C\ ^{16}O$ around 5 μm by Fourier spectroscopy under vacuum. J Mol Spectrosc 1979;75: 251–69.

[224] McClatchey RA, Benedict WS, Clough SA, Burch DE, Calfee RF, Fox K, et al. AFCRL Atmospheric absorption line parameters compilation. Technical report, AFCRL-TR-73-0096, Air Force Cambridge Research Laboratories; 1973.

[225] Rothman LS, Gordon IE, Barbe A, Benner DC, Bernath PF, Birk M, et al. The HITRAN 2008 molecular spectroscopic database. J Quant Spectrosc Radiat Transfer 2009;110:533–72.

[226] Gerstenkorn S, Luc P. Absolute iodine (I_2) standards measured by means of Fourier-transform spectroscopy. Rev Phys Appl 1979;14: 791–4.

[227] Tennyson J, Kostin MA, Barletta P, Harris GJ, Polyansky OL, Ramanlal J, et al. DVR3D: a program suite for the calculation of rotation–vibration spectra of triatomic molecules. Comput Phys Commun 2004;163:85–116.

[228] Polyansky OL, Zobov NF, Viti S, Tennyson J, Bernath PF, Wallace L. K band spectrum of water in sunspots. Astrophys J 1997;489: L205–8.

[229] Toth RA. SISAM database ⟨http://mark4sun.jpl.nasa.gov⟩ (2007).

[230] Rothman LS, Jacquemart D, Barbe A, Benner DC, Birk M, Brown LR, et al. The HITRAN 2004 molecular spectroscopic database. J Quant Spectrosc Radiat Transfer 2005;96:139–204.

[231] Gordon IE, Rothman LS, Gamache RR, Jacquemart D, Boone C, Bernath PF, et al. Current updates of the water-vapor line list in HITRAN: a new "diet" for air-broadened half-widths. J Quant Spectrosc Radiat Transfer 2007;108:389–402.

[232] Tennyson J, Yurchenko SN. ExoMol: molecular line lists for exoplanet and other atmospheres. Mon Not R Astron Soc 2012;425:21–33.

[233] Lodi L, Tennyson J. A linelist of allowed and forbidden rotational transitions for water. J Quant Spectrosc Radiat Transfer 2008;109: 1219–33.

[234] Lodi L, Tennyson J. Line lists for $H_2^{18}O$ and $H_2^{17}O$ based on empirically-adjusted line positions and ab initio intensities. J Quant Spectrosc Radiat Transfer 2012;113:850–8.

[235] Tallis L, Coleman M, Gardiner T, Ptashnik IV, Shine KP. Assessment of the consistency of H_2O line intensities over the near-infrared using sun-pointing ground-based Fourier transform spectroscopy. J Quant Spectrosc Radiat Transfer 2011;112:2268–80.

[236] Bykov AD, Fazliev AZ, Filippov NN, Kozodoev AV, Privezentsev AI, Sinitsa LN, et al. Distributed information system on atmospheric spectroscopy. Geophys Res Abstr 2007;9:01906 SRef-ID: 1607-7962/gra/EGU2007-A-01906.

[237] Császár AG, Fazliev AZ, Tennyson J. W@DIS—prototype information system for systematization of spectral data of water. In: Abstracts of the twentieth colloquium on high resolution molecular spectroscopy, ⟨http://vesta.u-bourgogne.fr/hrms/⟩; 2007.